U.PORTO

FEUP FACULDADE DE ENGENHARIA
UNIVERSIDADE DO PORTO

INTEGRATED MASTER IN ENVIRONMENTAL ENGINEERING 2019/2020

INFLUENCE OF THE SOLVENT IN THE PREPARATION OF PGM-FREE CATHODE GAS DIFFUSION ELECTRODES FOR PEMFC APPLICATION

MIGUEL GALAZ PIMENTA DE MATOS

Dissertation submitted for the degree of

MASTER ON ENVIRONMENTAL ENGINEERING

President of the jury:
Professor Cidália Botelho

_____

Supervisor at the University:
Professor Adélio Mendes

_____

Supervisor at DLR:
PhD student Krishan Talukdar

_____

October 2020

Acknowledgments

Firstly, I would like to thank both FEUP and DLR for their incentive towards international cooperation and partnership. There are those who preach about the importance of a global research network for the future of science, and those that actually invest in its creation. Thank you for being the latter. Secondly, thank you to the Erasmus+ program for its financial support, and to the staff of the International Relations Service of the University of Porto. Without their ebullient support, I would have drowned in a sea of nightmarishly unintelligible paperwork.

To Prof. Adélio Mendes, thank you for accepting to supervise this work.

A special thanks to the researchers and technicians at DLR, specifically to Siggy, who had the patience to correct all my rookie mistakes on the workbench; to Daniel, who helped me to feel motivated during the several scorching and meticulous hours of drop casting; and to Pawel, who made me feel welcomed and considered despite my position as a novice.

A warm thank you to Krishan, who despite being incredibly busy with his PhD and later with the Covid-19 pandemic and all it entailed, made me feel supported and gave me the tools to finish my thesis with something interesting to say. His supervision was the best I've had during my academic years, and will be forever kept as one of my fondest university memories.

To Francisco, I have nothing to say that he already does not know. He is my confrère, a comrade met by pure chance, and the best friend someone can have. May we never succumb to conformity, and may we never lose our inquisitiveness. As a fictional old friend once said: "All we have to decide is what to do with the time that is given us".

More than a thank you, I wish to recognize my father as the key teacher in my life. His lessons shall not be wasted in me, and will be forever retained in my heart. This I hold as a promise for as long as I breathe.

To my mother, for her continuous presence and support, particularly cherished and vital in strange times of seclusion and confinement. It is good to know that no matter what, there is someone constantly thinking in one's well-being.

There is no one more paramount in my life than you. You who needs not be named. You who gave me the gift of true happiness and caring. Who has been travelling with me for the past eight years in a land of muddle, stress and enigmas, never leaving my side. To you I cannot thank nor recognize, for that is too little. To you I give my heart, now and forever, despite all that may happen to ourselves and the world around us. You are my life, my purpose, my soul. May this be another step towards our freedom, and our final and permanent reunion.

Prof. Adélio Mendes, supervisor of this dissertation, is an integrated member of LEPABE – Laboratório de Engenharia de Processos, Ambiente Biotecnologia e Energia, financed by Financiamento Base - UIDB/00511/2020 da Unidade de Investigação – LEPABE – financed by national funds through FCT/MCTES (PIDDAC)

Abstract

Polymer electrolyte membrane fuel cell (PEMFC) technology has become a greener alternative to the combustion of fossil fuel. Platinum (used as catalyst) is one of the most expensive materials used in the manufacturing of PEMFC systems. To reduce the manufacturing cost of PEMFC, platinum group metal (PGM)-free catalysts draw interest in the electrochemical society. The type of solvent and ionomer content utilized to fabricate cathode catalyst layer (CCL) in a PGM-free PEMFC plays an important role in the fuel cell performance. The performance and durability of PGM-free cathode electrodes are still crucial for their wide commercialization. In this study, a catalyst belonging to the family of Fe-N-C materials was mixed with different solvents and ionomer ratios in ink suspensions for cathode electrode fabrication. Their performances were analyzed via membrane electrode assembly (MEA) single cell testing under H_2/Air operating conditions, and subsequently subjected to a potentiostatic hold stability test at 400 mV for 48 hours. Ink suspensions were further characterized by zeta-potential measurements.

A clear correlation was found between fuel cell performance and ionomer content and type of solvent used. Zeta-potential analysis allowed to comprehend the impact of particle dispersion in the performance of the electrode, in which there seems to exist an "optimal" balance between excessive or insufficient particle dispersion. Stability testing revealed that higher performing MEAs also suffer higher degradation rates, yet the main responsible mechanism remains unknown. For the solvent types and ionomer contents tested in this work, use of methanol at 50 weight percent (wt%) of ionomer content produced the highest peak power density (0.229 $W \cdot cm^{-2}$), which is comparable to the most recent state of the art PGM-free catalysts.

Keywords: **PEMFC, PGM-free catalyst, MEA characterization, ink suspension optimization, single cell testing**.

Resumo

A tecnologia de célula de combustível de membrana de electrólito de polímero (PEMFC) tornou-se uma alternativa mais ecológica em comparação com a queima de combustíveis fósseis. Platina (usada como catalisador) é um dos materiais mais caros utilizados no fabrico de sistemas PEMFC. Para reduzir o custo da produção de PEMFC, catalisadores sem metal do grupo da platina têm ganho interesse na sociedade eletroquímica.

O tipo de solvente e teor de ionómero utilizados na camada de catalisador catódico (CCL) de uma PEMFC isenta de metais do grupo da platina (PGM-free) cumprem um papel importante no desempenho da célula de combustível. Melhorias no desempenho e estabilidade dos elétrodos catódicos livres de metais preciosos são cruciais para a sua larga comercialização. Neste estudo, um catalisador pertencente à família dos materiais Fe-N-C foi misturado com diferentes solventes e proporções de ionómero em suspensões de tinta para o fabrico de eléctrodos catódicos. Os seus desempenhos foram analisados através da montagem de eléctrodos de membrana (MEA), por meio de testes de célula única em condições operacionais H_2/Ar e, subsequentemente, submetidos a um teste de estabilidade de retenção potenciostática a 400 mV durante 48 horas. As suspensões de tinta foram ainda caracterizadas através de medições de potencial zeta.

Uma correlação clara foi encontrada entre o desempenho da célula de combustível e o conteúdo de ionómero e o tipo de solvente utilizados. A análise do potencial zeta permitiu compreender o impacto da dispersão de partículas no desempenho do eléctrodo, onde parece existir um equilíbrio "óptimo" entre dispersão excessiva ou insuficiente de partículas. Os testes de estabilidade revelaram que MEAs de melhor desempenho também sofrem taxas de degradação mais altas, no entanto o principal mecanismo responsável por este fenómeno permanece desconhecido. Para os tipos de solvente e conteúdos de ionómero testados neste estudo, uso de metanol a 50 porcento em peso (wt%) de teor de ionómero produziu a maior densidade de potência de pico (0,229 $W \cdot cm^{-2}$), comparável ao mais recente estado da arte para catalisadores PGM-free.

Declaration

I hereby declare, under word of honor, that this work is original and that all non-original contributions are indicated and due reference is given to the author and source

Miguel Galat Pimenta de Matos

September 2020

Index

List of Figures ix

List of Tables xi

Notation and Glossary xiii

1 Introduction 1

1.1 Motivation 1

1.2 Presentation of the Research Institute 2

1.3 Contribution of the author to the work 3

1.4 Organization of the thesis 4

2 Context and State of the Art 5

2.1 Fuel Cell 5

2.2 Polymer Electrolyte Membrane Fuel Cells 5

2.3 Fuel Cell Thermodynamics and Performance 8

2.4 Surface Charge Analysis 11

2.5 Low- and Non-Platinum Catalysts Synthesis and Activity 12

2.6 Durability of PGM-free Electrodes 15

3 Materials and Methods 19

3.1 Materials 19

3.2 Methods 19

4 Results and discussion 23

4.1 Zeta-Potential 23

4.2 Fuel cell performance test 25

4.3 Zeta-Potential VS Fuel cell performance 27
4.4 Cyclic Voltammetry 28
4.5 Electrochemical Impedance Spectroscopy 30
4.6 Stability testing 32

5 Conclusions 35

6 Assessment of the work done 37

7 References 39

List of Figures

Figure 1. Basic operation of a Polymer Electrolyte Membrane Fuel Cell 6

Figure 2. Schematic representation of the components of a single PEMFC 8

Figure 3. Schematic of a PEMFC i-V curve. Three major losses occur in a fuel cell: Activation polarization, Ohmic polarization, and Concentration polarization (In 24).....9

Figure 4. Zeta-potential values of the produced inks, measured by mixing 100 µL of ink and 5000 µL of H_2O: a) Inks prepared with ethanol; b) Inks prepared with isopropyl alcohol; c) Inks prepared with methanol 24

Figure 5. H_2/Air polarization curves at different ionomer contents with: a) Ethanol; b) Isopropyl alcohol; c) Methanol 26

Figure 6. Cyclic voltammograms at different ionomer contents with: a) Ethanol; b) Isopropyl alcohol; c) Methanol 29

Figure 7. Nyquist plots from EIS measured at different ionomer contents with: a) Ethanol; b) Isopropyl alcohol; c) Methanol 31

Figure 8. Potentiostatic hold test at 400 mV for MEAs prepared with: a) 60 wt% ionomer with Ethanol; b) 50 wt% ionomer with Isopropyl alcohol; c) 50 wt% ionomer with Methanol 33

List of Tables

Table 1. Stability of the solution depending on the zeta-potential (Adapted from 25) 11

Table 2. Characterization of recent carbon-based PGM-free catalysts used in H_2/Air PEMFC under 80ºC 14

Table 3. Electrode Capacitance of the MEAs prepared at different ionomer content with ethanol, isopropyl alcohol or methanol 28

Notation and Glossary

Symbols and Units

Latin letters

C_E	Electrode Capacitance	$F \cdot cm^{-2}$
E	Electrical Potential difference	V
E_0	Reversible Potential	V
F	Faraday's constant	$C \cdot mol^{-1}$
G	Gibbs free energy	J
i	Current density	$A \cdot m^{-2}$
i_0	Exchange current density	$A \cdot m^{-2}$
R_c	Cell resistance	Ω
T	Absolute temperature	K
W_{elec}	Electrical work	V
$wt\%$	Weight percent	
Z	Impedance	Ω

Greek letters

α	Charge transfer coefficient	
ε_0	Permittivity of vacuum	
ε_r	Relative permittivity	
ζ	Zeta-Potential	V
η_{act}	Activation polarization	V
η_{con}	Concentration polarization	V
η_{ohm}	Ohmic polarization	V
μ_e	Electrophoretic mobility	$m^2 \cdot s^{-1} \cdot V^{-1}$
i	Current density	$A \cdot m^{-2}$
i_0	Exchange current density	$A \cdot m^{-2}$
R_c	Cell resistance	Ω
T	Absolute temperature	K
W_{elec}	Electrical work	V
$wt\%$	Weight percentage	
ζ	Impedance	Ω
ν	Scan-rate	$V \cdot s^{-1}$

List of Acronyms

ACL	Anode Catalyst Layer
BOT	Beginning Of Test
CCL	Cathode Catalyst Layer
CIE	Catalyst Imbued Electrode
CL	Catalyst Layer
CV	Cyclic Voltammetry
DLR	Deutsches Zentrum für Luft- und Raumfahrt
EDL	Electric Double Layer
EIS	Electrochemical Impedance Spectroscopy
EOT	End Of Test
FIB	Focused Ion Beam
GDE	Gas Diffusion Electrode
GDL	Gas Diffusion Layer
GHG	Greenhouse Gas
HOR	Hydrogen Oxidation Reaction
IEA	International Energy Agency
MEA	Membrane Electrode Assembly
MOF	Metal-Organic Framework
OCV	Open Circuit Voltage
ORR	Oxygen Reduction Reaction
PEM	Polymer Electrolyte Membrane
PEMFC	Polymer Electrolyte Membrane Fuel Cell
PGM	Precious Group Metal
RDE	Rotating Disk Electrode
TEM	Transmission Electron Microscope
STP	Standard Temperature and Pressure

1 Introduction

1.1 Motivation

The currently increasing energy demand and resources depletion due to high consumption have led to the development of new systems able to provide renewable and clean energy. Renewable energy sources such as wind and solar energy have been receiving more attention, being able to reduce global greenhouse gas (GHG) emissions and putting a strain on the current climate change threat. The Paris Agreement of 2015 aimed to strengthen the global response to this century temperature rise, by keeping it below the 1.5 degree Celsius mark. According to the scenario projected by the International Energy Agency (IEA), the global renewable share of energy production will increase from 6,777 TWh in 2018 to 26,065 TWh in 2040 (a 385 % increase). While this scenario translates into a higher contribution from renewable energy to power society's activities, there is still a huge dependency on fossil fuel energy (ca. 145,885 TWh in 2018, according to IEA), which is being exhausted at an alarming rate – at the current extraction rhythm, oil reserves will last approximately 50 more years (1). Therefore, both the environment and the global energy supply are at risk if fossil fuel continues to be the main source for energy production, with renewable energy being the best option as the future main energy source. Unfortunately, hydro, solar and wind power sources are intermittent (2), and energy storage methods to compensate for such fluctuations are still lacking. This has the potential to affect the economic value of renewable energies, making them unfeasible and/or incapable to fulfill the society's energy demands.

A promising solution lies within electrochemical applications, including fuel cells. Fuel cell technology is the nowadays most promising form of producing clean energy without the emission of GHGs. First created by the British scientist Sir William Grove in 1839) (3), fuel cells are electrochemical devices able to convert chemical energy from a fuel and an oxidizing agent into electricity (4). Recently, hydrogen was considered a sustainable energy source (5), and the production of H_2 by water electrolysis emerged as a promising solution for energy storage (6), mitigating the problem concerning the intermittency of renewable sources' energy production. Hydrogen may be utilized as fuel for a fuel cell, enabling the production of efficient energy at a steady rate (4, 5).

Fuel cells can be used for both stationary and mobile applications. Examples include: portable power, including laptops, cellular phones, and power tools; backup power, for example for computer systems; transportation, including automobiles, buses, and bicycles; stationary power

applications, often used to power houses not connected to the grid or to provide supplemental power. In particular, polymer electrolyte membrane fuel cells (PEMFCs) are a readily available alternative power source to combustion engines powered by fossil fuels, due to their high efficiency, fast start-up time and continuous operational capacity (4).

To achieve the worldwide commercialization of PEMFCs, several technological barriers must be surpassed, including performance issues, low durability under real operating conditions and water management (3, 4, 7). Also, practice of platinum as a catalyst in a fuel cell stack incurs in high economical costs (8). Eliminating precious group free metals is a significant challenge for fuel cell applications, and an important aspect for a more economically approachable use of this technology. Catalysts made of Fe-N-C coordinated structures are an acceptable alternative to precious group free metal catalysts. Performance optimization of fuel cells employing these catalysts depends on various parameters such as the thermal treatment of the catalyst, ionomer ratio, coating technique and operating conditions (such as inlet gas flows and operating temperature) (9).

This work aims to develop an optimized ink suspension of a Fe-N-C catalyst, specifically by optimizing the ionomer/catalyst ratio and solvent used in the ink preparation, alongside the development of an optimized membrane electrode assembly (MEA). The performance differences between the constructed MEAs are discussed in terms of the active surface area of the catalyst, determined by Cyclic Voltammetry (CV) (10, 11), and by the proton resistance through the catalyst layer, measured by Electrochemical Impedance Spectroscopy (EIS) (12). Furthermore, Zeta-Potential measurements for each produced ink suspension were run to analyse the stability and agglomeration of the catalyst particles in the suspension (13).

1.2 Presentation of the Research Institute

The Deutsches Zentrum für Luft- und Raumfahrt (DLR) is the national aeronautics and space research center of the Federal Republic of Germany. Its extensive research and development work in the fields of aeronautics, space, energy, transport, security and digitalization is integrated into national and international cooperative ventures. DLR is also responsible for the planning and implementation of Germany's space activities on behalf of the federal government. Furthermore, DLR is the umbrella organization for one of Germany's largest project management agencies.

The DLR institute of Engineering Thermodynamics in Stuttgart, with additional research facilities in Cologne, Ulm, Oldenburg and Hamburg, conducts research in the field of efficient energy storage systems that conserve natural resources and next generation energy conversion technologies, with a staff of 180 scientific and technical employees, engineers and doctoral students. The spectrum of activities ranges from theoretical studies to laboratory work for basic research and operation of pilot plants. These experimental and theoretical studies are accompanied by system analysis studies to evaluate the associated technological, environmental and economic potential, and situate it in a larger overall context of the energy economy.

1.3 Contribution of the author to the work

The goal of this project was to optimize membrane electrode assemblies' fabrication utilizing a Fe-N-C (Platinum group metal free) catalyst, via polarization curve and cyclic voltammetry (CV) and electrochemical impedance spectroscopy (EIS) analysis, as well as zeta-potential measurements of the produced inks. Stability tests were run with the best performing membrane electrode assemblies.

The author was responsible for the optimization of ionomer ratios and solvents utilized in the ink preparation, following the currently practiced methodologies for both ink preparation and casting on the gas diffusion layers. Towards reaching the recommended compression rate of the membrane electrode assemblies, the author also optimized the torque pressure applied during the hot-press stage.

Polarization curves were drawn after the recommended conditioning stage, following the advised three-minute interval between measurements and the operating conditions discussed between the author and the DLR supervisor. CV and EIS were measured according to the recommended settings for Fe-N-C catalyst based electrodes, obtained and analyzed by the author.

Stability test settings were defined by the author according to the recently published work regarding degradation-related phenomena on fuel cells. Measurements were registered and analyzed by the author.

Zeta-potential settings were discussed between the author and the DLR supervisor, and ink preparation and measuring were completed by the author. Data analysis was of the author's responsibility.

1.4 Organization of the thesis

This work is divided into six chapters. Chapter 1, Introduction, gives a framework for the importance of this field of research towards the ultimate goal of producing clean and renewable energy. Presentation of the company in which the work was completed and its main objectives are also referred.

Chapter 2, Context and State-of-the-art, provides information regarding the principles behind fuel cell technology and describes preceding studies.

Chapter 3, Materials and Methods, gives a detailed description of the materials and equipment utilized, and the experimental procedures.

Chapter 4, Results and Discussion, consists of a full analysis of the experimental results, presenting and examining each of the performed tests.

Chapter 5, Conclusions, presents the main key points reached during this work.

Finally, chapter 6, Assessment of the work done, states the rate of completion for each objective presented in chapter 1, and the author's personal opinion for the performance and achievements of the performed work.

2 Context and State of the Art

2.1 Fuel Cell

A fuel cell may be regarded as a galvanic cell, taking fuel and oxidant as inputs and producing electricity as output. As long as the inputs are being provided, it will continuously generate electricity (14). Thus, a fuel cell is an energy conversion system that transforms chemical energy into electrical energy.

The main advantage of a fuel cell when compared with combustion engines is its higher efficiency of energy conversion, and lower noise and chemical pollution. A fuel cell produces electricity directly from chemical energy, while a combustion engine needs first to burn the fuel (converting chemical energy to heat), convert heat into mechanical energy, and only then produce electricity (15). Fuel cells are primarily classified according to the type of electrolyte they employ. This classification determines the electro-chemical reactions that occur in the cell, the type of catalyst required, the temperature range in which the cell operates, the necessary fuel, among other factors (16). Several types of fuel cells are currently under development, namely Alkaline Fuel Cells, Direct Methanol Fuel Cells, Molten Carbonate Fuel Cells, Phosphoric Acid Fuel Cells, Solid Oxide Fuel Cells, and Polymer Electrolyte Membrane Fuel Cells (4, 16).

2.2 Polymer Electrolyte Membrane Fuel Cells

Considering a polymer electrolyte membrane fuel cell (PEMFC), electricity is produced directly by harnessing the electrons of the H_2 molecules, as they move from high-energy reactant bonds to low-energy product bonds (H_2O molecules). By spatially separating the H_2 and O_2 reactants, extending the length necessary for the electrons to cross to complete the electron transfer and the bonding reconfiguration, they can be harnessed to create an electrical current (4). This reaction is split into two electrochemical half reactions:

$$H_2 \leftrightarrow 2H^+ + 2e^- \qquad \text{(HOR)} \tag{2.1}$$

$$\frac{1}{2}O_2 + 2H^+ + 2e^- \leftrightarrow H_2O \qquad \text{(ORR)} \tag{2.2}$$

These half reactions are named hydrogen oxidation reaction (HOR) and oxygen reduction reaction (ORR), respectively (3). It is their spatial separation that allows the flow of electrons

through an external circuit and the production of electrical current. In order to create this separation an electrolyte must be employed. In the 1950's, ion-exchange membranes were invented as electrolytes for fuel cells (17). They consist in thin layers of material that allow ions to flow through them, impeding the passage of electrons (4). Consequently, the electrons are forced to travel across the external circuit, while the ions flow through the electrolyte from the anode to the cathode side (Figure 1).

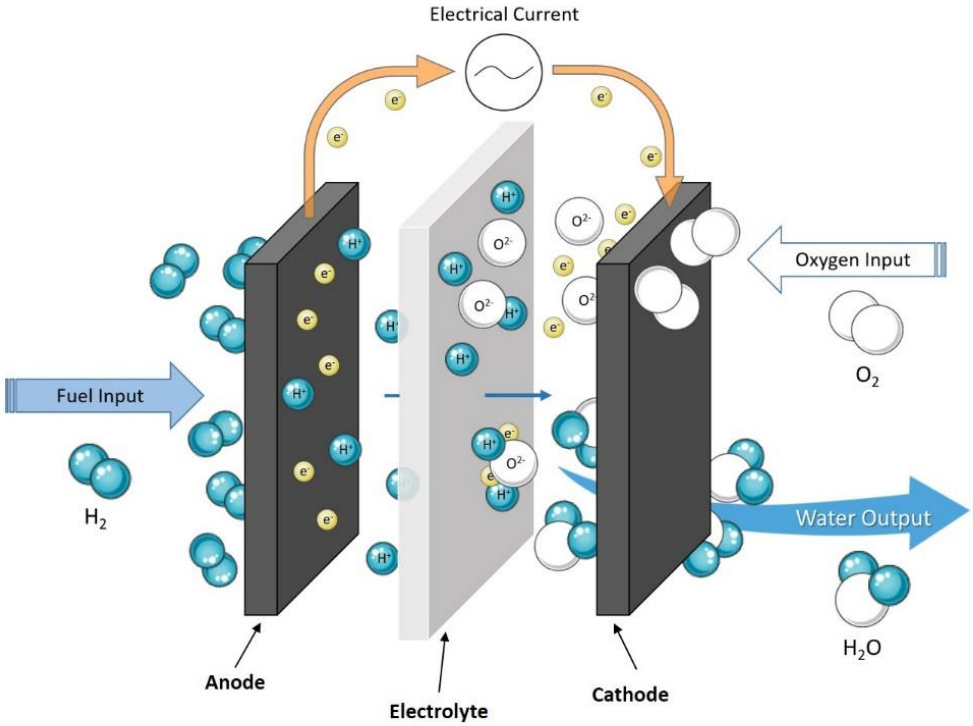

Figure 1. Basic operation of a Polymer Electrolyte Membrane Fuel Cell. Hydrogen enters the cell, where it is oxidized by the Anode Catalyst Layer (ACL), giving protons (H^+) and electrons (e^-). Electrons flow through the external circuit, generating electrical current, while protons flow through the Electrolyte. On the Cathode Catalyst Layer (CCL) ORR occurs and, ultimately, water is formed by recombination of the protons, electrons and oxygen ions (O^{2-}). Produced water is removed from the cell to prevent flooding.

PEMFCs have been developed for transportation, portable devices, and combined heat and power systems (7). In addition to not producing pollutants while working, PEMFCs have efficiencies of around 60 % for electrical energy conversion and 80 % for cogeneration of electrical and thermal energies (14). Compared to other fuel cells, they are not at risk for electrolyte leakage, have a short warm-up time, low operating temperature (usually 80°C), easy scale-up, and high power density (7, 18). The main reasons that hinder a more global usage of this technology lie with the high-cost and low durability of PEMFCs, along with the need for hydrogen production and fuel station infrastructures (3).

A PEMFC comprises at least two electrodes: an anode where oxidation takes place and a cathode where reduction occurs. These electrodes, called gas diffusion electrodes (GDEs), consist of two parts: a catalyst layer (CL), with an usual thickness of 5 – 30 μm, and a gas diffusion layer (GDL), with a 100 – 300 μm thickness, that allows for an even distribution and transport of reactants to the catalyst layer (17). The CL is composed by a catalyst, a carbon substrate, a hydrophobic substance and Nafion® or other ionomer that promotes proton conductivity, while the GDL is a mixture of carbon, water, alcohol and a hydrophobic substance (19). In addition, the fuel cell includes an electrolyte to control the flow of ions and electrons, an external circuit to collect the electrical current, a fuel plus oxidant intake, and a water output (4).

PEMFCs employ a thin proton conducting polymer membrane as the electrolyte, commonly made of Nafion®, a state-of-the-art ionomer composed of a hydrophobic polymer backbone and hydrophilic ionized side-chains, and catalyst imbued electrodes (CIE) (3, 20). The purpose of the ionomer is to facilitate proton transport, increasing hydrophobicity and avoiding flooding in the cell (19). The most relevant part of a PEMFC is its polymer electrolyte membrane (PEM), made to be as thin as possible (under 100 μm) while maintaining its impermeability to reactive gases, its mechanical stability, and being non-electrically conducting (3, 21). A CIE, made of carbon fiber paper or carbon cloth coated with catalyst, is bonded to each side of the PEM (14). The union of the PEM with both CIEs creates a membrane electrode assembly (MEA) (3).

Both the anode and cathode of a PEMFC have highly dispersed catalyst nanoparticles (4). Currently, the state-of-the-art catalyst is made of platinum – Pt/C (7). Pt nanoparticles on carbon black GDL are used on the anode and cathode sides of a PEMFC (17), with loadings of <0.05 $mg \cdot cm^{-2}$ and >0.4 $mg \cdot cm^{-2}$, respectively (22). Catalyst loading on the anode side is less than on the cathode side due to the reactions simplicity: HOR is fast and straightforward, while ORR is sluggish, requiring many individual stages and molecular reorganizations (4). Oxygen reduction to water necessitates the transfer of four electrons and four protons, which occur sequentially (17). This transfer can happen by different reaction pathways, creating a complex network of individual steps and intermediates. Furthermore, H_2O_2 molecules that may be formed are corrosive and accelerate catalyst and membrane degradation, thus decreasing the fuel cell efficiency (17).

Once the MEA fabrication is finished, the fuel cell can be assembled. To do so, a gasket is employed on both the ACL and CCL side of the MEA, which allow for the control of the compression rate and avoid gas leakage (21). On top of these an anode and cathode flow field plates are assembled, allowing for a laminar flow of reactants across the fuel cell (23). These have elaborate flow structures comprised of small flow channels that promote uniform mixing

and distribution (4). Finally, an end plate is fixed at the end of both flow plates, keeping all the structures together and allowing heating and current drawing from the fuel cell (23). Figure 2 shows a schematic representation of the components of a single PEMFC.

The overall electrochemical reaction occurring inside a single working PEMFC is as follows:

$$H_2 + \frac{1}{2}O_2 \leftrightarrow H_2O + \text{Electricity} + \text{Heat} \tag{2.3}$$

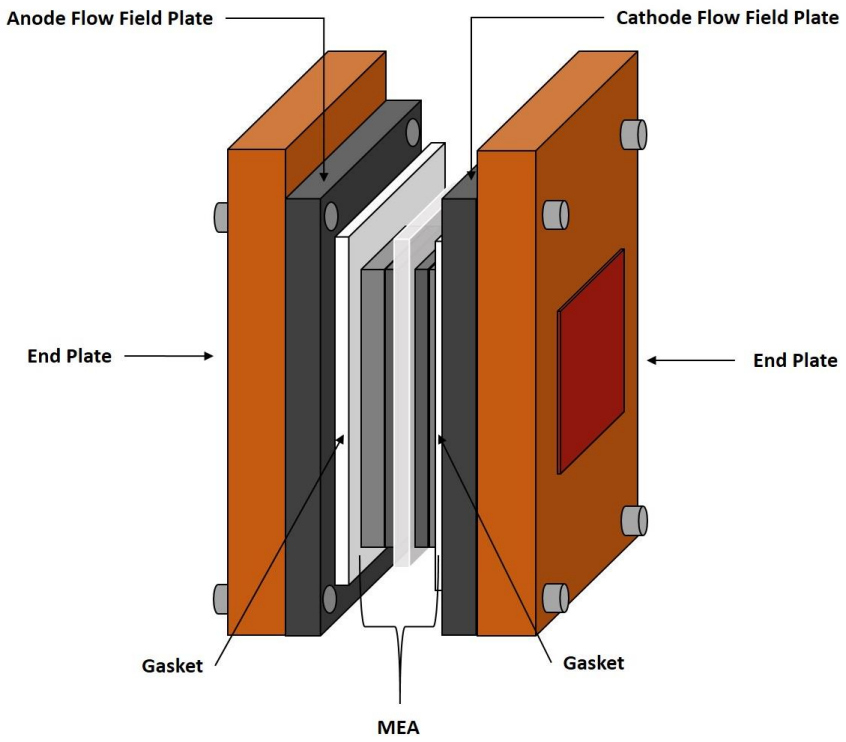

Figure 2. Schematic representation of the components of a single PEMFC.

2.3 Fuel Cell Thermodynamics and Performance

A fuel cell's performance is influenced by thermodynamic variables such as pressure, temperature, and gas concentration (24). The aim of a fuel cell is to extract the internal energy from a fuel and transform it into electrical work (W_{elec}). Considering the HOR and ORR occurring in a PEMFC, the maximum work output that can be obtained relates to the Gibbs free energy (G) change, which represents the exploitable energy potential of the system at constant temperature and pressure (24). In a general sense, G can be seen as the energy required to create a system and make room for it, minus the energy provided by the environment due to heat transfer (4). Thus, since the potential of a system to perform W_{elec} is measured by its voltage (V), G sets the magnitude of the reversible voltage for an electrochemical reaction:

$$W_{elec} = \Delta G = -nFE \tag{2.4}$$

where n is the number of moles of electrons transferred, F is Faraday's constant, and E is the electrical potential difference.

At standard temperature and pressure conditions (STP; 25°C and atmospheric pressure), the reversible voltage (E_0) is 1,23 V, *i.e.,* the highest voltage obtainable from an H_2-O_2 fuel cell under these conditions (4). To determine the ideal performance of the fuel cell operating under real working conditions (80°C for PEMFCs), the Nernst potential can be applied, represented by cell voltage (24). For an H_2-O_2 PEMFC, the Nernst equation to determine the reversible voltage at real operating temperature and pressure (E) is

$$E = E_0 - \frac{RT}{2F} ln \left[\frac{1}{P_{H_2} P_{O_2}^{1/2}} \right] \tag{2.5}$$

where R is the universal gas constant, T the absolute temperature, and P the gas pressure.

From this equation, it is possible to conclude that an increase of the reactant gases pressure will improve the reversible voltage. Besides improving the system's efficiency, increasing the pressure also reduces electrolyte loss by evaporation (24).

By connecting a PEMFC to a workbench it is possible to draw electrical energy from it and to measure its performance through a plot of its current-voltage characteristics – called an i-V or polarization curve (4). Current values are given according to a referenced area ($A \cdot cm^{-2}$) to standardize the effects of the system size, allowing for comparison between fuel cells (3, 4). A typical polarization curve of a PEMFC has a shape similar to the one in Figure 3, encompassing three major types of performance loss, also called polarizations.

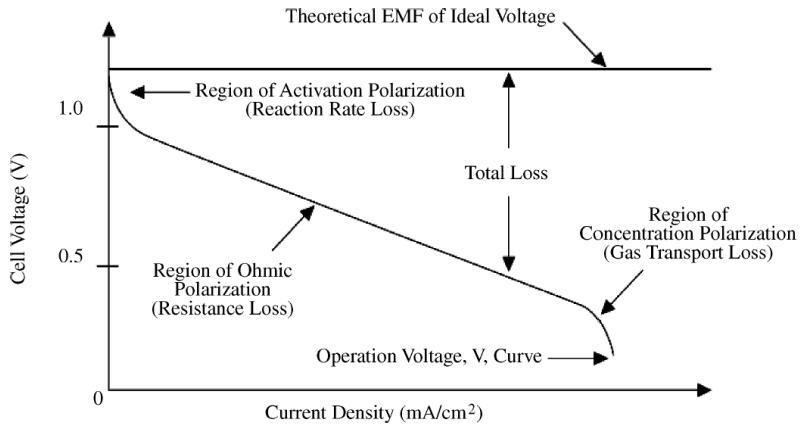

Figure 3. Schematic of a PEMFC i-V curve. Three major losses occur in a fuel cell: Activation polarization, Ohmic polarization, and Concentration polarization (in 24).

Concentration polarization occurs due to the change of the reactant concentration at the surface of the electrodes, as fuel is being consumed. Higher current outputs lead to higher concentration losses (3). If a fuel cell works at real operating current densities, slow transport of reactants and removal of products becomes a major contribution for concentration polarization (24). Concentration loss can be represented by the following equation:

$$\eta_{con} = \left(\frac{RT}{nF}\right) \ln\left(1 - \frac{i}{i_{\Delta}}\right) \tag{2.6}$$

where i_{Δ} is the limiting current density, *i.e.*, the maximum achievable current density. Concentration losses can occur due to several processes, including sluggish diffusion of the gas phase in the electrode pores, solution of reactants into the electrolyte, dissolution of products out of the system, and diffusion of reactants and products through the electrolyte (24).

Ohmic polarization is the direct resistance to the flow of charge and ions through the electrodes and the electrolyte, respectively, and it can be influenced by the structure and dimension of the electrolyte, water content on the cell, temperature and catalyst loading (3). Ohmic loss can be represented by

$$\eta_{ohm} = iR_c \tag{2.7}$$

where R_c is cell resistance. The majority of ohmic losses occur in the electrolyte, which can be reduced by decreasing the electrode separation, enhancing electrolyte ion conductivity or by changing the electrolyte's properties (24). The voltage drop is proportional to the current density, and linear (3).

The electrical energy produced by a fuel cell depends on the rate of the electrochemical half reactions, *i.e.*, the production and consumption of charge. In order for reactants to convert to products, they need to first overcome an activation barrier in order to reach an activated state (24). The prospect that a reactant can overcome that barrier determines the rate of the reaction. To lower the activation barrier, a portion of voltage is sacrificed, a phenomenon called activation overvoltage, η_{act}, that increases the rate of reactant conversion and the current density output of the fuel cell (4). The process of sacrificing voltage to lower the activation barrier is named Activation polarization, and can be represented by

$$\eta_{act} = \left(\frac{RT}{\alpha nF}\right) \ln\left(\frac{i}{i_0}\right) \tag{2.8}$$

where α is the charge transfer coefficient and i_0 the exchange current density. Activation losses are governed by reaction conditions plus the catalyst's material and nanostructure, which can lead to a low active surface area (17).

By subtracting these losses from the ideal performance of the fuel cell, the real performance can be obtained, ultimately representing the amount of electrical energy that can be produced. In normal practice, the operation of a fuel cell is referred to by its power density (in $mW \cdot cm^{-2}$), which is obtained by multiplying the current density and cell voltage in each point of the i-V curve (4). The chosen operating value should be inferior to the peak power density, yielding a compromise between current output, fuel cell stability, lifetime and operating costs (24).

2.4 Surface Charge Analysis

Nanoparticles have a specific charge on their surface area which attracts a small layer of ions (named Stern layer). This double layer of surface ions and attracted ions travels with the nanoparticle as it disperses in the solution (13). The electrical potential at the boundary of the double layer is named zeta-potential of the particles and has values that range from +100 mV to -100 mV (25). The magnitude of the zeta-potential value provides a good index of the colloidal stability of the solution, meaning the electrostatic repulsion between charged particles (13). Generally, nanoparticles with a zeta-potential value higher than +30 mV or lower than -30 mV have high levels of stability. Dispersions with values between +25 mV and -25 mV eventually agglomerate due to particle interactions such as van der Waals and hydrophobic interactions and hydrogen bonding (25). Zeta-potential analysis is therefore an important tool for understanding the surface characteristics of a nanoparticle and predicting its stability in the solution. The stability behaviour of the solution is dependent on the zeta potential as follows:

Table 1. Stability of the solution depending on the zeta-potential (Adapted from 25)

Zeta-Potential (mV)	**Stability Behaviour**
0 to ± 5	Quick Flocculation
± 10 to ± 30	Emergent Instability
± 30 to ± 40	Relative Stability
± 40 to ± 60	Good Stability
> 61	Excellent Stability

Zeta-potential is calculated by using theoretical models and experimentally determined electrophoretic mobility. In this work electrophoretic light scattering, which can be used to characterize nanoparticles, was utilized. Applying an electric field through a dispersion creates particle migration towards the electrode with opposite charge, whose velocity is proportional to the magnitude of the zeta-potential, determined by the dispersant viscosity and dielectric constant according to Smoluchowvski's equation (13):

$$\mu_e = \frac{\varepsilon_r \varepsilon_0 \zeta}{\eta(T)} \tag{2.9}$$

where μ_e is the electrophoretic mobility, ε_r the dielectric constant (relative permittivity), ε_0 the permittivity of vacuum, $\eta(T)$ the dispersant viscosity (function of temperature), and ζ the zeta-potential.

2.5 Low- and Non-Platinum Catalysts Synthesis and Activity

There has been significant progress towards the reduction of Pt loadings on fuel cells, as well as methods for platinum recovery from PEMFCs (7, 26). However, low availability and high demand lead to a continuous increase in Pt costs – the current global demand of platinum is approximately 200 tons per year, while estimated available reserves are of 40 kilotons (27). This offsets the efforts to reduce the Pt content and hinders wide commercialization of PEMFCs, by ultimately creating unsustainable costs (28). Indeed, the US Department of Energy projected that Pt-based catalysts represent approximately half the cost of an automotive fuel cell stack (29).

While Pt is the best candidate for anode catalyst layer (ACL) and cathode catalyst layer (CCL) construction, its reduction or complete elimination while maintaining high cell performances, especially on the thicker CCL, would bring significant improvements cost-wise. Development of new catalysts and optimization of MEA construction are crucial steps towards this objective and the main point of focus of recent research efforts.

New catalyst synthesis must consider the Sabatier principle, where a reactant must bind strongly enough to the catalyst for the reaction to occur yet weakly enough so that the product will disassociate and the catalyst surface does not become poisoned by reactant intermediates (30, 31). Morphology and shape of the catalyst nanoparticles also play an important role in the catalytic activity (30). On the other hand, MEA optimization is related with the design of the electrode layer (32). Performance differences between PEMFCs are not only influenced by the intrinsic activity of the catalyst, but also by the active-site accessibility, aggregate level of diffusion, mass transport properties and proton resistance through the catalyst layer (CL) (33).

In turn, these properties are related with the ionomer distribution over the CL, which is influenced by the deposition method and ionomer content of the prepared ink (32).

For the past 12 years intensive research efforts have been made towards developing low- and non-platinum catalysts that can perform as well or better than their Pt/C counterparts (7, 17, 22, 29, 34). These include Pt alloys, core-shell structures, Pd-based catalysts, non-PGM transition metal based catalysts, and carbon based non-noble metal catalysts (7).

So far, the highest observed activities were of Pt alloys and core-shell structures (35, 36). Indeed, it has been confirmed that Pt alloys, with proper post-treatment, have better activity and durability in PEMFC than Pt/C (37). Also, core-shell structures, synthesized by depositing a thin Pt-based shell around a less expensive core (such as Pd-based nanoparticles), have shown high mass activities (35). While promising, ink and catalyst layer composition, and preparation techniques have not yet been optimized for core-shell structure catalysts and require further research. Furthermore, both Pt alloys' and core-shell structures' highest ORR activities were obtained via rotating disk electrode (RDE) measurements and require real fuel cell testing to ascertain their feasibility in fuel cell applications (7).

Non-PGM transition metal based catalysts, *i.e.*, metal oxides, nitrides, oxynitrides and carbonitrides, were proposed as catalyst supports to replace carbon. Metal oxides are chemically stable under acidic electrolytes, yet show low activity associated with low electrical conductivity and deficiency in adsorption sites for O_2 species on the metal oxides' surface (38). Metal nitrides and oxynitrides are generally less active than metal oxides, which is also related with low electrical conductivity (7). The onset potential of metal carbonitrides is highly dependent on the content of N atoms. Nevertheless, while an increase in N content from 0 % to 3 % showed significant increases of the onset potential (22), they are still not superior to their metal nitrides counterparts. Despite the significant progress towards increasing non-PGM transition metal catalysts' performance, their activity is still not comparable to that of Pt-based catalysts (7).

Carbon-based PGM-free materials containing Fe and N atoms (Fe-N-C catalysts) are another possible replacement for Pt at the cathode of a PEMFC (39). They are produced via pyrolysis of a Fe precursor, an N precursor and a carbon support at high temperature (7). The interest for Fe-N-C catalysts has been increasing due to their encouraging catalytic activity and the use of abundant and low-cost precursors for their synthesis (34, 39-43). Indeed, recent improvements of Fe-N-C catalysts performance and durability led to the commercialization of the first PEMFC portable device utilizing this type of catalyst – the NPMC-based FCgen®-1040, a fuel cell stack generator created by Ballard Power Systems (44). However, PEMFCs for automotive usage require higher power densities, which have not yet been reached. High performing Fe-N-C

catalysts synthesis is varied, still they are subjected at least to one high temperature pyrolysis, between 800°C and 1000°C (32). The ink preparation for MEA construction also follows different recipes, mainly regarding the weight ratio of ionomer to catalyst loaded at the cathode side and the type of solvent used. Moreover, thickness of the membrane, fuel cell temperature, gas nature (H_2/O_2 or H_2/Air flow) and humidity, and back pressure are relevant variables for cell performance testing (7). Therefore, it is difficult to compare the published performance results for carbon-based non-PGM catalysts. Nevertheless, it is ascertained that the most common factor to obtaining a high performing catalyst is the use of a carbon precursor like a metal-organic framework (MOF) (7). While most studies tested cell performance under H_2/O_2 conditions, H_2/Air represents real operating conditions, since in automotive practice the source of O_2 is ambient air (15). It should be noted that switching from O_2 to air may reduce the peak power density of the cell by a factor of 2 (7). Under H_2/Air and at 80°C, recent high performing carbon--based catalysts synthesized with a carbon precursor are displayed in Table 2.

Table 2. Characterization of recent carbon-based PGM-free catalysts used in H_2/Air PEMFC under 80°C

Catalyst's Name	Peak Power Density ($W \cdot cm^{-2}$)	Ink Composition (wt% Nafion® – wt% catalyst)	Solvent used	Cathode Loading ($mg \cdot cm^{-2}$)	Coating Technique	Active Surface Area (m^2/g)	Back pressure (atm)	Reference
Pajarito Powder®	0.37	50 – 50	Isopropyl Alcohol	3.0	Automatic Spraying	N/A	2.5	(34)
TPI(SiO_2)-650-C	0.42	50 – 50	Isopropyl Alcohol	1.0	Brushing	650	1.0	(43)
Fe-N/CDC	0.24	50 – 50	Ethanol	4.0	Drop Casting	945	1.0	(45)
(CM + PANI)-Fe-C	0.39	65 – 35	Isopropyl Alcohol	4.0	Brushing	1500	1.0	(46)
Fe-MSG	0.25	55 – 45	Isopropyl Alcohol	4.0	Hand Spraying	N/A	1.4	(47)
Black Pearl 2000 C support	0.33	65 – 35	Isopropyl Alcohol	4.8	Brushing	350	1.0	(9)

For the mentioned fuel cell tests, it is noticeable that 1) utilizing isopropyl alcohol as solvent is the most general practice, with the single result using ethanol showing lower peak power density; 2) brushing and automatic spraying coating techniques provided higher performances, most likely due to a more homogeneous deposition of ink on the GDE; and 3) changes in the ink composition (weight percentage (wt%) of ionomer and catalyst) and active surface area of the

catalysts do not seem to directly relate to performance differences, meaning they may be influenced by the type of catalyst's synthesis.

Currently, the low volumetric activity of PGM-free catalysts requires higher loadings and thicker electrodes than their Pt counterparts, so that they can have acceptable performances. A PGM-free CCL can be 5-10 times thicker than a state-of-the-art Pt/C CCL, causing higher mass transport resistances and limiting the voltage obtained at high current densities (41). CCL thickness and catalyst loading can be lowered if the intrinsic activity of PGM-free catalysts improves, *i.e.,* there is an increase in the active sites density, but limitations challenge this improvement (44). The overall performance of a PGM-free fuel cell is influenced by a number of variables, such as the intrinsic activity and loading of the catalyst, ionomer content (32), ink composition, concentration and dispersion (48), methods for the electrode fabrication (49) and drying settings (50). While catalyst loading and ionomer content are proven to play an important role (51, 52), the other parameters' influence is less clear (32).

Moreover, although studies are being carried towards developing innovative Fe-N-C catalysts (7, 39, 41), CCL development and optimization of MEA assemblies is a crucial, albeit less frequently approached, research aspect (19).

2.6 Durability of PGM-free Electrodes

Currently, the instability of PGM-free catalysts is the greatest challenge for their commercial implementation in PEMFCs (53). A typical fuel cell with a PGM-free cathode degrades between 40 and 80 % in the first 100 hours of testing, which tends to be more noticeable for catalysts with higher initial activity (54). For a portable device, the minimum requirements are 1000 working hours with less than 10 % performance loss, while 5000 working hours are a prerequisite for motive applications (55).

The most active sites for ORR in M-N-C catalysts (M being Fe, Co, or Mn) are viewed as metal centres coordinated by nitrogen atoms bound to a carbon matrix – called MN_x moieties, plausibly hosted by micro- (< 2 nm in diameter) and mesopores in the carbon (46, 53, 56). These MN_x moieties catalyse the transfer of the first $2e^-$ during the ORR (57). According to Shao Y. *et al*. (2016), initial performance and degradation rate of PGM-free cathodes on PEMFCs are closely related to micropores, with a larger micropore surface area leading to better initial performance and higher degradation rate. Another influencing factor is the higher quantity of H_2O_2 produced on PGM-free catalysts via the Fenton reaction, when compared to PGM ones (58). This is probably due to the lower catalytic activity of the PGM-free active sites for O-O bond scission,

alongside the possibility of carbon playing a role in H_2O_2 formation. Furthermore, the latter tends to increase with the reduction of the catalyst loading (57).

PGM-free cathode degradation is often divided in two phases: Phase I in the first few to 20 hours of testing and Phase II after the 20th hour (53). The biggest performance losses happen within the first 20 hours, while Phase II testing shows slower performance degradation with relatively stable current densities (59-61). Phase I was more frequently studied since it seems to be more important than Phase II, and their study less time-consuming (53).

Four mechanisms are proposed for the degradation of PGM-free cathodes: micropore flooding; protonation of active sites and/or basic N moieties next to the active sites; demetallation; and carbon oxidation (53, 55, 59, 61-63).

As mentioned, micropores host many active sites in PGM-free catalysts, and therefore their flooding may influence the cell's performance since the sites for ORR become obstructed. Nevertheless, according to Chenitz R. *et al*. (2018) and Banham D. *et al*. (2017), this is not responsible for the fast performance decay in the Phase I of the catalyst's lifetime.

Protonation of nitrogen atoms means that the lone electron pair on the pyridinic-N can bind protons in the cathode of a PEMFC, leading to ORR inactive sites and loss of performance (64). However, this was not confirmed for distinct catalysts (65). Also, a recent work unsuccessfully attempted to prove the existence of the composite FeN_4-N active sites and their inactivation (66). Therefore, active site protonation followed by anion adsorption is still not yet proved to be a main degradation mechanism.

MN_x moieties are the most likely active sites for the ORR in a well-performing M-N-C catalyst (53). Demetallation of PGM-free catalysts, *i.e.,* the breaking of the substrate and the metal atom, promotes leaching of the transition-metal ions, which are almost always detrimental to the fuel cell's performance, mainly due to catalyst degradation and because they can catalyse the deterioration of the membrane and ionomer in the CL (53). Chenitz *et al.* (2018) proposed that Fe-N_4 active sites, according to the Le Chatelier principle, demetallate in the flux of water running in the micropores, leading to a fast current decay in Phase I. A correlation between the number of Fe-N_4 sites and current density was also observed, providing for a strong argument in favour of specific demetallation of MN_4 moieties in the micropores. However, since most PGM-free catalysts are currently acid-washed before incorporating into the CCL (63), most of the leachable iron atoms should be removed and not affect the cell performance for the first several hours (63, 67).

M-N-C catalysts have a highly disordered carbon phase, likely to promote anodic oxidation of the catalyst (53). At 0.9 or higher voltages, Choi CH. *et al.* (2015) detected a CO_2 evolution during the carbon electrochemical oxidation. Furthermore, it is reasonably speculated that electrochemical carbon oxidation to oxygen-containing functional groups takes place at or below 0.9 V (61). Carbon oxidation, accelerated at higher potentials, may result in the destruction of MN_4 active sites, leading to decreased ORR activity and structural damage of the cell (53).

Alongside electrochemical oxidation at high potentials, chemical oxidation by H_2O_2 can also occur, mainly due to the already stated higher peroxide generation of PGM-free catalysts. Catalyst degradation by H_2O_2 attacks leads to a decrease in ORR activity, especially in acidic PEMFC, caused by the formation of reactive oxygen species responsible for carbon oxidation (68). Chemical oxidation of carbon next to MN_4 sites may also lead to the sites' demetallation and to structural disintegration of the catalyst layer (34). While carbon electrochemical oxidation happens below 0.9 V, carbon chemical oxidation by H_2O_2 occurs close to 0.3 V (where H_2O_2 is also formed) (53).

According to Banham D. *et al.* (2017), there is a correlation between catalyst loading and fuel cell stability. The authors stated that since most of the ORR takes place near the interface between membrane and CCL, most of the catalyst oxidation should also take place near this interface. As catalyst oxidation progresses, the ORR zone moves deeper into the CCL, where non-oxidized catalyst is still available. Upon testing different catalyst loadings for 60 hours under galvanostatic mode, a higher catalyst loading of 4.0 $mg \cdot cm^{-2}$ led to a performance loss of approximately 10 %, while a loading of 1.0 $mg \cdot cm^{-2}$ led to a loss of 55 %. In this sense, a CCL with higher catalyst loading will run out of non-oxidized catalyst later than one with a lower catalyst loading.

Chenitz *et al*. (2018) tested seven MEAs under H_2/Air for 125 hours with a potential range between 0.8 V and 0.2 V. According to their results, changing the potential of the performed chrono-amperometry does not seem to affect the change in the current density of the MEA when the polarization curve is drawn, *i.e.*, the shape of the decay curve is similar whichever the potential used. Yet, it was noted that during Phase I the slope of relative change in the mean current density is steeper for higher potentials. Additionally, they conducted Neutron activation analysis, concluding that the cause of the initial fast decay of current density is the complete demetallation of the Fe-N_4-like sites located in the micropores, due to the Le Chatelier principle, which might be related to the high porosity of the catalyst they used (>1000 m^2/g).

The formation of H_2O_2 radicals is dependent on operating conditions such as cell temperature, relative humidity and current output (58). Nosaka *et al.* (69) tested the influence of each of these conditions on a Pt/C catalyst, concluding that 1) the higher the cell temperature, the more

H_2O_2 radicals are formed, because Nafion® softens, increasing gas crossleak; 2) the lower the gas humidity, the higher the amount of H_2O_2 radicals formed, since H_2O_2 remains in the membrane due to its higher boiling point; 3) the lower the operating current, the higher the amount of H_2O_2 radicals formed.

In summary, while there is no general consensus regarding the factors that truly influence a PGM-free fuel cell's stability, demetallation and carbon oxidation by H_2O_2 formation seem to be the main mechanisms behind the degradation of PGM-free fuel cells. Demetallation of Fe-N_4 sites might be dependent on the porosity of the catalyst, while H_2O_2 formation and consequent carbon corrosion can be influenced by operating conditions, such as cell temperature, relative humidity, and current, and by the electrode fabrication. To the best of the author's knowledge, ionomer ratio and type of solvent used in the ink fabrication stage have not been related with stability changes, nor if they influence the mechanisms described above.

3 Materials and Methods

3.1 Materials

The PGM-free catalyst used in this work was a commercial Fe-N-C material with an average 10 nm pore size (Pajarito Powder®, LLC). Ninety-nine percent ethanol, isopropyl alcohol and methanol (Sigma-Aldrich) were used as solvents, depending on the desired MEA. A 10 weight percentage (wt%) Nafion® solution (DuPont Inc.) was used as ionomer. Prepared inks were ultrasonicated in a Bandelin Sonocool 255 unit and probe sonicated in a 50 Hz UP200S Hielscher probe ultrasonicator unit.

Inks were drop-casted over a hot-plate with disposable 10 mL syringes onto Sigracet 25 BC non-woven carbon paper GDL (SGL carbon GmBH) with an average thickness of 225 μm. A commercial Pt/C GDE with a loading of 0.3 $mg_{Pt} \cdot cm^{-2}$ was used as anode, with an average thickness of 235 μm. MEAs were fabricated using Nafion® XL membrane (Ion Power) with an average thickness of 28 μm. MEAs were assembled onto a single cell with golden coated SS bipolar plates and two meander three serpentine channel graphite flow fields (DLR). Teflon gaskets were used on the anode and cathode side of the MEAs, with 180 μm and 230 μm in thickness, respectively. A home-made workstation (DLR) was used for performance testing. Cyclic Voltammetry (CV) and Electrochemical Impedance Spectroscopy (EIS) were performed and recorded with a Zahner potentiostat.

Zeta-potentials were measured with a Malvern Panalytical ZetaSizer Advance Range unit. Prepared inks were injected into a Malvern Panalytical INC DTS1070 folded capillary cell, using disposable 20 mL syringes.

3.2 Methods

Ink preparation. PGM-free catalyst inks were prepared by mixing 15 mg of catalyst with a desired amount of dispersing solvent (ethanol, isopropyl alcohol or methanol) and Nafion® ionomer, in order to obtain 40, 50 or 60 wt% ionomer content in the dry electrode. The resulting ink was ultrasonicated for 10 min in a 20°C bath, probe sonicated for 5 min at 0.5 cycles and at 40 % amplitude, and finally ultrasonicated for another 30 min in a 20°C bath.

Single cell testing. In order to determine the performance that the produced inks could attain, single cell performance tests were conducted. To prepare the cathode, each fabricated ink was

deposited onto a 1.69 cm^2 square of Sigracet 25 BC GDL with a disposable syringe over a hot-plate at 100°C. The drop-casting followed a sequential pattern of four drops for each of the four rows/columns necessary to completely embed the GDL. After each row/column was filled, the drops were left to dry before casting the following row/column. Once four rows were complete, the procedure was repeated for four columns, and vice-versa. This cycle was repeated until reaching a total desired catalyst loading of 3.5 $mg \cdot cm^{-2}$, measured by calculating the difference between the weight of the GDL before and after the drop-casting. As for the anode, commercial Pt/C GDE was used, with a loading of 0.3 $mg_{Pt} \cdot cm^{-2}$, also with a total area of 1.69 cm^2. The prepared cathode and anode were hot-pressed onto each side of a Nafion® XL membrane at 125°C for 5 min, under torque pressure of 2.0 N.m to obtain a desired compression rate of 13 %. The prepared MEA was then assembled by framing it with a Teflon gasket, on each side, on a single cell, and analyzed in a home-made workstation. The cell was run at 80°C under a feed of saturated H_2/Air (100 % relative humidity) at 200 and 400 sccm, respectively, and pressurized to a total of 2.5 atm_{gauge}. Conditioning of the cell for > 4 hours under potentiostatic and galvanostatic mode was performed before recording the polarization curves. Polarization curves were recorded in galvanostatic mode starting at stable open circuit voltage (OCV) and until reaching the first potential value below 200 mV, holding each current rate for 3 min before taking the average voltage of the last 30 s. Two polarization curves were recorded for each MEA, and the average value considered. This procedure was similar for each of the inks prepared.

Electrochemical Impedance Spectroscopy (EIS) testing. EIS evaluation allows to measure the proton resistance in the CCL, giving information about the connectivity of ionomer pathways for proton transport. EIS was measured at 80°C cell temperature under saturated H_2/Air flow at 200 and 400 sccm, respectively, at 2.5 atm_{gauge}. Frequency ranged between 10,000 and 0.1 Hz, starting at 1,000 Hz. Two measurements were performed for each MEA, at current densities of 100 mA (at 5 mA of amplitude) and 600 mA (at 30 mA of amplitude). This allowed to analyze the proton resistance of the CCL in the activation polarization region and in the ohmic polarization region of the polarization curves, respectively.

Cyclic Voltammetry (CV) testing. The performance of an MEA is related to the catalyst surface chemistry and the electrode level interactions. Running CV tests on the produced MEAs allows for the obtaining of capacitive responses, which give information about those characteristics, specifically between ionomer and catalyst. After single cell testing, the MEAs were purged with a nitrogen flow on the cathode side and hydrogen flow on the anode side, both at 1,000 sccm. CV values were obtained using a potentiostat, measured at 80°C fuel cell temperature under H_2/N_2

flow (both at 80 sccm) at 2.5 atm_{gauge}. Three cycling potentials were run for each MEA between potential scan ranges of 0.06 and 1.0 V, at a scan rate of 0.02 $V \cdot s^{-1}$. Towards determining the electrode capacitance, current values at 0.4 V in the anodic direction (where the adsorbed H_2 is oxidized to H^+) and in the cathodic direction (reduction of H^+ to H_2) were considered. Electrode capacitance was calculated according to the following equation:

$$C_E = \frac{i_{CV,+}^{0.4V} + |i_{CV,-}^{0.4V}|}{2v} \tag{3.1}$$

where v is the scan rate (in $V \cdot s^{-1}$), $i_{CV,+}^{0.4V}$ is the current value at 0.4 V on the positive (anodic) direction (in $mA \cdot cm^{-2}$), and $i_{CV,-}^{0.4V}$ is the current value at 0.4 V on the negative (cathodic) direction (in $mA \cdot cm^{-2}$).

Zeta-Potential testing. Zeta-Potential measurements offer a good magnitude index of the repulsive interaction between particles in a dispersion, useful to assess their stability. In this sense, a high zeta-potential value translates to a high resistance to aggregation. For each produced ink, 100 µL of ink were mixed with 5,000 µL of distilled water, sonicated for 2 min in a 25°C bath, and injected into a DTS1070 folded capillary cell. Ink to water concentration was chosen so that there were enough light scattering events in the solution but no decrease in the intensity of the scattered light due to high ink concentration (25). The capillary cell was then inserted into the ZetaSizer. Six measurements were performed at 25°C for each ink, defining the dispersant as water and a refractive index absorption of 1.59.

Stability testing. Stability tests were executed at 80°C under a feed of saturated H_2/Air at 200 and 400 sccm, respectively, and pressurized to a total of 2.5 atm_{gauge}. Conditioning for 2 hours was performed previous to the start of testing. The cells were then subjected for 48 hours to a potentiostatic hold test at 400 mV. Automatic recording of current density output was registered every 5 seconds.

4 Results and discussion

4.1 Zeta-Potential

The type and composition of the dispersing solvent influences the homogeneity of the produced ink, and in turn the catalyst agglomerates size on the CL (70). Also, the type of solvent influences the structure of the ionomer dispersed in the ink, ultimately affecting its distribution on the CCL and the fuel cell performance (71). A sufficiently high level of repulsion between the particles in an ink suspension is important to produce a good catalyst dispersion in the electrode (13). The smaller the particle agglomerations, the higher the amount of catalyst available for the reaction to occur. In this sense, it is expected that a good performing cathode can be related with the casting of an ink solution with high zeta-potential value.

Nine ink solutions were prepared with different solvents and ionomer ratios. Ethanol, isopropyl alcohol and methanol were used, and ionomer contents of 40, 50 and 60 wt% were tested for each solvent. The average value of the six zeta-potential measurements applied for each ink are shown in Figures 4a, 4b and 4c.

According to the relation between the zeta-potential and the stability behavior of the solution, displayed on Table 1, all the prepared inks showed good or excellent stability (< -40 mV). Ethanol seems to produce a very well dispersed solution, with values reaching under -60 mV, translating into an excellent dispersion of the particles in the ink. Moreover, a higher ionomer content of 60 wt% promotes slightly less catalyst dispersion in the ink (-63.3 mV), yet still reaching excellent stability. The use of isopropyl alcohol as solvent led to the lowest obtained zeta-potentials (between -55.0 mV and -52.0 mV), meaning a good stability behavior of the ink. Compared with ethanol, isopropyl alcohol produces solutions with a higher level of agglomeration, which might decrease the performance of MEAs when utilizing this solvent in their manufacture. Differences in the ionomer content do not seem to affect the obtained zeta-potential values, with only a 3 mV difference between inks prepared with 60 and 40 wt% of Nafion®. Lastly, inks prepared with methanol present zeta-potential values between the other two solvents (-61.8 mV to -57.4 mV). As with ethanol, this means that methanol promotes an excellent stability behavior of the prepared solution, yet a lower overall zeta-potential may translate into less performance of MEAs prepared with methanol. Contrary to ethanol, a smaller ionomer content seems to promote more catalyst agglomeration in the ink.

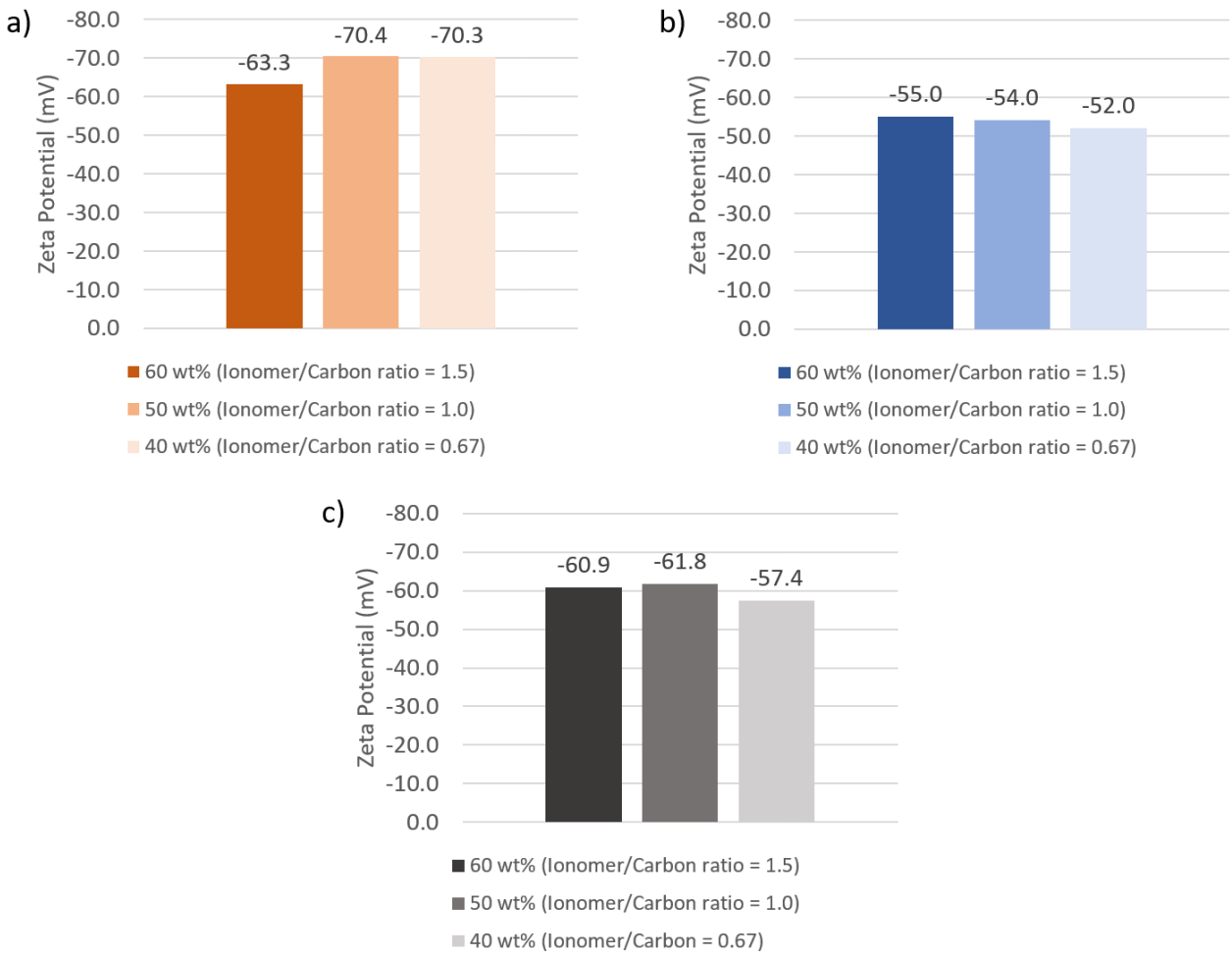

Figure 4. Zeta-potential values of the produced inks, measured by mixing 100 µL of ink and 5000 µL of H_2O: a) Inks prepared with ethanol; b) Inks prepared with isopropyl alcohol; c) Inks prepared with methanol.

Polymers such as Nafion® seem to increase the stability of colloidal solutions by steric repulsion (repulsive forces between intersecting electron clouds) (20). Therefore, an absence of ionomer leads to a lack of steric repulsion forces, leading to particle agglomeration. This was true for the inks prepared with isopropyl alcohol and methanol, where a lower ionomer content led to a lower zeta-potential, and so theoretically higher agglomeration. In opposition, the same did not happen with ethanol, and zeta-potential differences with different ionomer contents of the previous two solvents are slight.

Electric double layer (EDL) forces keep the particles of a colloid solution separated, increasing its stability (13). When there is a lack of ionomer EDL forces appear as a secondary stability mechanism, due to the deficiency of sulfonate groups of the Nafion® polymer chain, replacing steric repulsion (20). EDL forces are able to explain the higher dispersion with lower ionomer content of inks prepared with ethanol, yet the same did not occur for the other solvents.

Following the Smoluchowvski's equation (see 2.9), it is expected that a higher dielectric constant of the solvent causes higher zeta-potential values and lower agglomerations. It has been shown that high dielectric constants are advantageous for cell performance (72). However, while isopropyl alcohol has the lowest dielectric constant (ε_r = 17.9) and presented lower zeta-potentials, both ethanol (ε_r = 24.5) and methanol (ε_r = 32.7) did not follow this trend.

Zeta-potential analysis by itself does not allow to fully understand the impact of the solvent in the preparation of a PGM-free cathode. In this sense, fuel cell performance tests were run with each prepared ink, in order to understand its impact on the current output of the cell.

4.2 Fuel cell performance test

To achieve good fuel cell performance, an optimal ionomer content must be assured. In order to lower the proton resistance of the CCL, a sufficiently high ionomer loading is required (32), and it differs between the catalyst and fabrication methods used (70). However, increased ionomer loadings may result in higher mass transport resistances through the electrode, due to the higher thickness of PGM-free electrodes (9). As stated above, the solvent type influences the homogeneity of the ionomer distribution in the CCL and thus the fuel cell performance due to lower proton conductivity throughout the CL.

For this study, MEAs were prepared utilizing the same PGM-free catalyst, changing the solvent (ethanol, isopropyl alcohol or methanol) and the ionomer content (60, 50 or 40 wt%) of the cathode ink. All cathode electrodes had the same catalyst loading of 3.5 mg·cm^{-2} ± 6 %. Figures 5a, 5b and 5c show the H_2/Air polarization curves of MEAs using cathodes prepared at different ionomer ratios with ethanol, isopropyl alcohol and methanol, respectively.

Using ethanol, the MEA with 60 wt% of ionomer performs better, reaching a peak power density of 0.210 W·cm^{-2}. The lower the ionomer content, the poorer the performance (0.177 and 0.142 W·cm^{-2}, respectively for 50 and 40 wt%). Using isopropyl alcohol, 50 wt% of ionomer performs the best, while a higher or lower ionomer content seemed to decrease current output. Compared with ethanol, the peak power density was considerably lower even by the best performing MEA (0.161 W·cm^{-2} for 50 wt%). Methanol performed the best at 50 wt% ionomer content, reaching 0.229 W·cm^{-2} and outperforming the MEAs prepared with ethanol. A lower ionomer content of 40 wt% performed slightly better at high current density, reaching a similar peak power density of 0.225 W·cm^{-2}. A higher ionomer content performs worse for methanol (0.199 W·cm^{-2}).

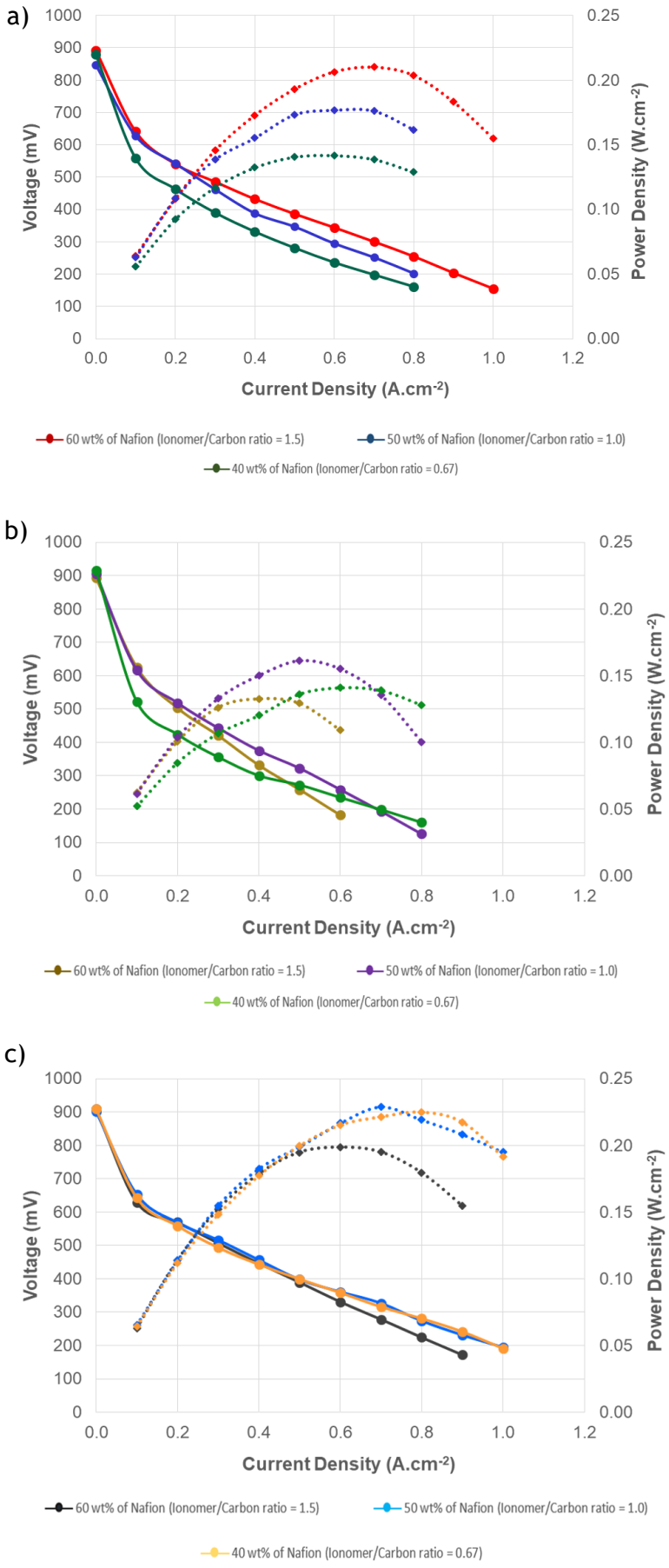

Figure 5. H_2/Air polarization curves at different ionomer contents with: a) Ethanol; b) Isopropyl alcohol; c) Methanol.

While there is a clear "optimum" ionomer content for each solvent used under the specific fabrication method described in this work, it is difficult to assess proton and mass transport contributions for voltage loss from a polarization curve. Also, while isopropyl alcohol clearly performed worse, ethanol and methanol allowed for similar peak power densities. In order to understand the impact of ink fabrication for fuel cell performance, a correlation between the previous zeta-potential analysis and the polarization curves must be approached. Furthermore, proton conductivity and mass transport through the electrode are analysed via electrochemical *in situ* diagnostics to elucidate the motive behind the range of obtained performances.

4.3 Zeta-Potential VS Fuel cell performance

As stated above, a lack of ionomer leads to a lack of steric repulsion, compensated by EDL forces. Inks prepared with ethanol seemed to prove this phenomenon. However, the higher zeta-potentials with lower ionomer contents produced the lower power densities (see Figure 5). A combination of high zeta-potential (-70.3 mV) and low ionomer content (40 wt%) produced the lowest peak power density for inks prepared with ethanol (0.142 $W \cdot cm^{-2}$). Contrarily, for isopropyl alcohol and methanol lower ionomer contents translated into lower zeta-potentials, albeit slightly. Although isopropyl alcohol showed low peak power densities compared to the other two solvents, methanol performed the best at 50 wt%, and similarly at 40 wt%. While zeta-potential decreased for the lower ionomer content, power densities remained high. A possible explanation for this phenomenon relates to the degree of particle dispersion in the ink. If too low, particle dispersion leads to catalyst agglomeration and less available active area, while when too high, dispersion leads to ionomer straining and eventually breakage of proton conducting pathways. This may be related with the lower power densities of ethanol at 50 and 40 wt% of ionomer, since a higher particle dispersion required a higher ionomer loading to mitigate strainings. Therefore it can be stated that an "optimal" zeta-potential value should be ensured. Considering the preparation method and PGM-free catalyst used in this work, to reach a peak power density of and above 0.200 $W \cdot cm^{-2}$, cathode ink zeta-potential should be somewhere in the range of -57 mV and -64 mV. This supposition requires further diagnostics such as transmission electron microscope (TEM) observations, which allows to assess the morphology of Nafion® molecules in solutions (72). Such analysis would allow to understand the real impact of particle dispersion in the ionomer distribution throughout the electrode and confirm the "optimal" zeta-potential value range proposed in this work.

4.4 Cyclic Voltammetry

CVs for electrodes manufactured with ethanol, isopropyl alcohol and methanol, and corresponding ionomer contents, are shown in Figures 6a, 6b and 6c, respectively. CV analysis allows to obtain information about the electrode level interactions between ionomer and catalyst (32). The shape of the cyclic voltammograms in Figures 6a, 6b and 6c is quasi-rectangular, meaning that the main contributor for the capacitive current is the electrostatic charge and discharge of the double layer (73). The same catalyst loading and fabrication method were used for all the MEAs, and therefore capacitance differences are related with variations in the microstructure of the electrode (32). Electrode capacitance of each MEA, *i.e.*, its electric charge, are shown in Table 3, determined by Eq. 3.1.

Table 3. Electrode Capacitance of the MEAs prepared at different ionomer content with ethanol, isopropyl alcohol or methanol

Nafion® content (wt%)	**Electrode Capacitance ($mF \cdot cm^{-2}$)**		
	Ethanol	**Isopropyl Alcohol**	**Methanol**
60	384.15	391.58	165.38
50	307.55	164.13	303.00
40	342.55	288.18	264.43

MEAs prepared with ethanol obtained the highest average capacitance. Regardless of ionomer content, values exceeded 300 $mF \cdot cm^{-2}$. While at 60 wt% the highest capacitance and power densities were obtained, at other ionomer contents capacitance differences were not steep. This may be explained by an enhanced interaction between ionomer and catalyst, due to the increased coverage of catalyst surface promoted by ethanol, which in turn increased the capacitive response. Nevertheless, a higher amount of ionomer facilitates the coverage of the catalyst, also increasing the capacitive response of the electrode. The same is valid for isopropyl alcohol, which reached its highest capacitance at higher ionomer content. However, at 50 wt% the lowest capacitance and highest power densities were obtained, contradicting the relation between high capacitance and high performance. In order to comprehend the causes behind this condition, further studies are needed. Finally, methanol had a higher capacitance and performance at 50 wt%. While electrode capacitance was lower than with ethanol, performance was slightly higher. A higher ionomer content provides more surface coverage of the catalyst, yet can lead to higher mass transport resistances. This could explain the performance differences between ethanol and methanol.

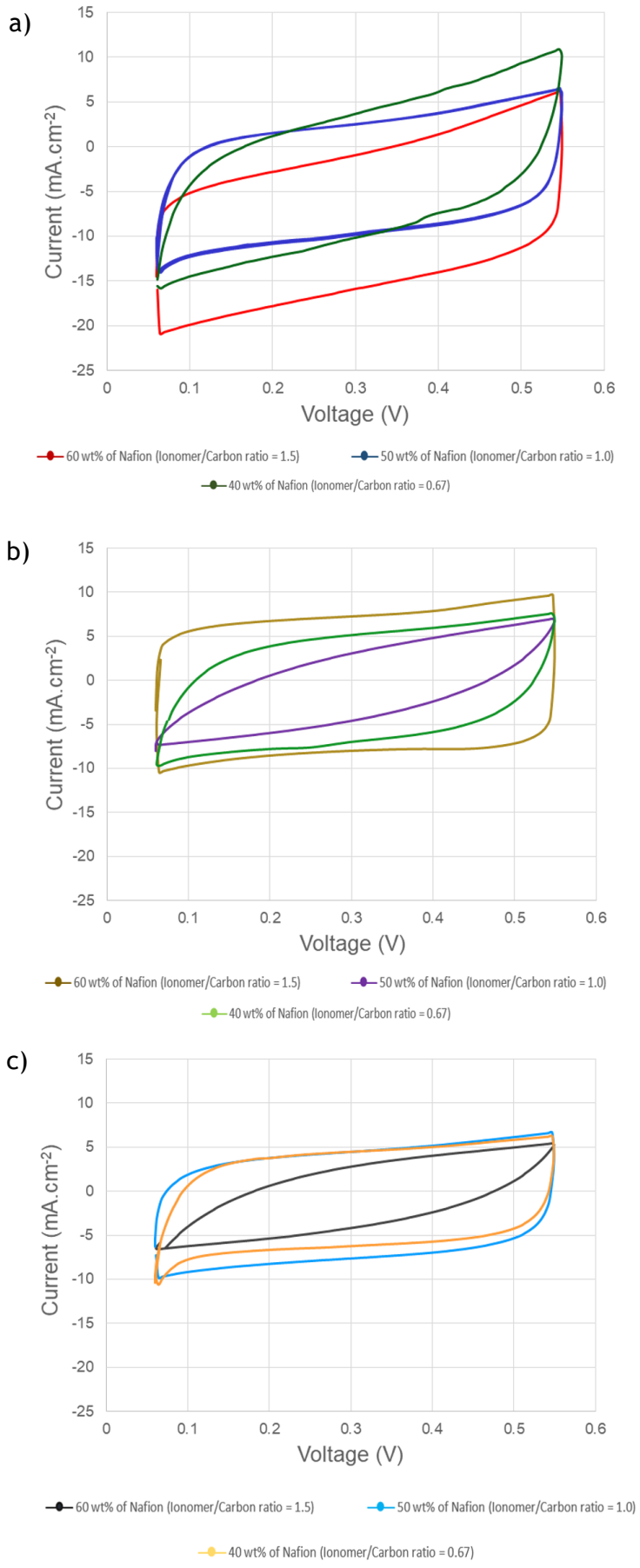

Figure 6. Cyclic voltammograms at different ionomer contents with: a) Ethanol; b) Isopropyl alcohol; c) Methanol.

4.5 Electrochemical Impedance Spectroscopy

EIS measurements were conducted at 100 mA and 600 mA in order to, respectively, evaluate the contribution of activation and ohmic resistances in the electrode performance. Concentration resistances were not analyzed due to the size and power output of the fuel cell. Figures 7a, 7b and 7c show the Nyquist plots at 100 mA and 600 mA for each MEA prepared with ethanol, isopropyl alcohol and methanol, respectively, and at different ionomer contents.

At 100 mA, the activation polarization is predominant, where in order for reactants to convert to products they need to first overcome an activation barrier to reach an activated state. At this current density, the MEA prepared with ethanol and 40 wt% of ionomer had the highest impedance, meaning the highest resistance. Indeed, at this current density the MEA had the lowest power density of the experiments with ethanol. The same occurred with isopropyl alcohol, in which a lower ionomer content promoted higher activation resistances. For MEAs prepared with methanol activation resistance remained similar throughout the practiced range of ionomer contents, causing the lowest performance impacts amongst all experiments. By observing the Nyquist plots in Figures 7a, 7b and 7c, it can be stated that a higher ionomer content leads to lower activations resistances. This tendency may be explained by the higher electrode capacitance at higher ionomer loadings, leading to an increased active surface area.

Ohmic polarization, *i.e.*, the resistance to the flow of charge and ions through the electrodes and the electrolyte, is predominant at higher currents. At 600 mA, MEAs prepared with ethanol have slightly higher charge resistances at 50 wt% ionomer content. At 40 wt% impedance was lowest, correlating with the fact that for PGM-free catalysts increased ionomer contents lead to increased charge resistances. However, the increased active surface area seems to compensate for charge resistances, explaining the better performance of the MEA with 60 wt% of ionomer. It was not possible to test the isopropyl alcohol MEA at 60 wt% due to the low voltage at 600 mA (under 200 mV), which would have damaged the MEA. At 50 wt% there was a considerably higher charge resistance than at 40 wt%, again compensated by the lower activation resistance. The same was seen for methanol, leading to the conclusion that while higher ionomer loadings resulted in higher charge resistances, the decreased activation resistances are not only able to compensate for such output losses, but they origin higher performances of the MEA.

Of the three tested solvents, considering the utilized fabrication method, methanol prompts the lowest impedances obtained. At low current densities this can be explained by the already stated higher dielectric constant of methanol and the zeta-potential range for the prepared inks, which leads to an “optimal” active surface area in the electrode.

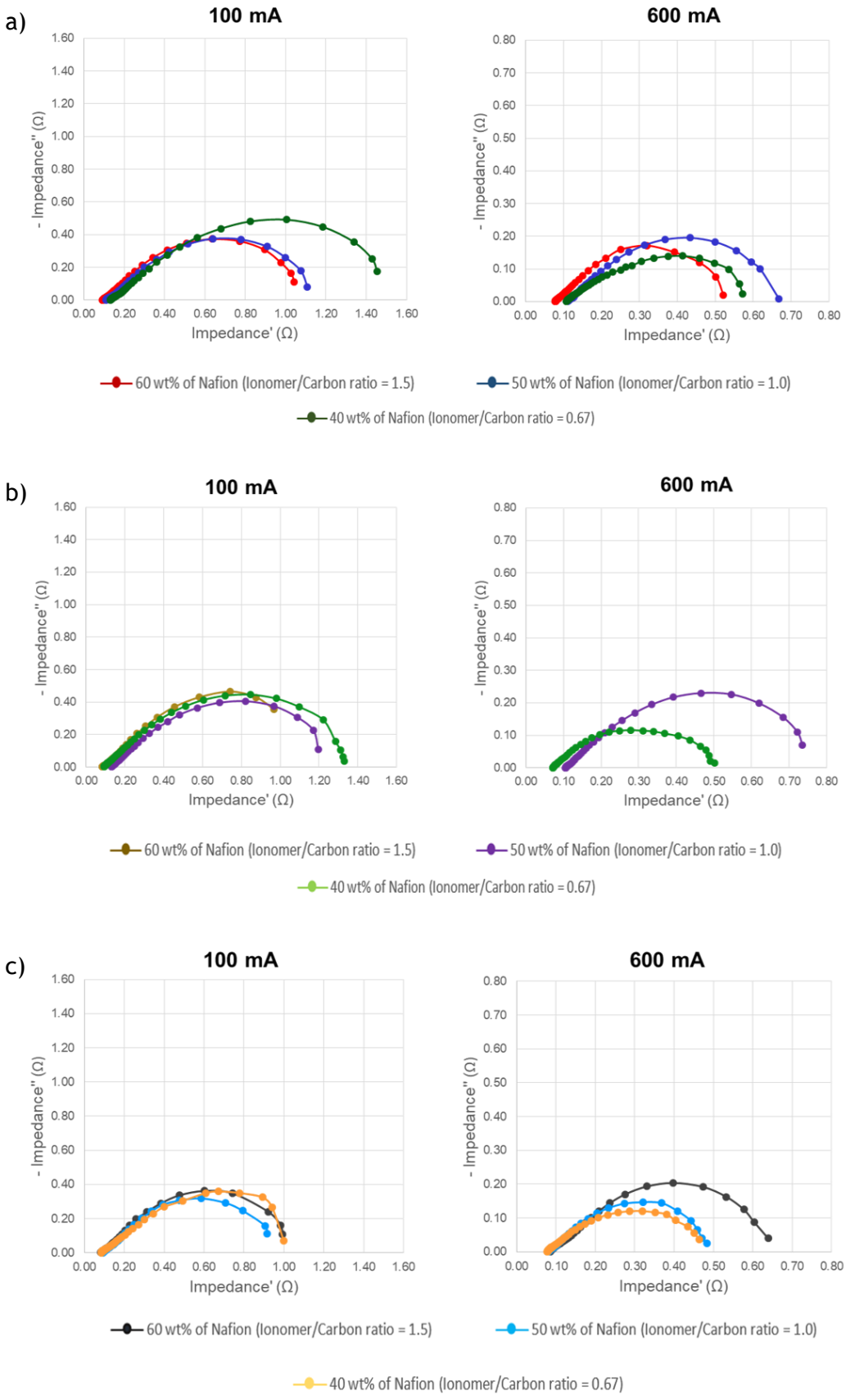

Figure 7. Nyquist plots from EIS measured at different ionomer contents with: a) Ethanol; b) Isopropyl alcohol; c) Methanol.

4.6 Stability testing

For each solvent tested, the best performing MEA was subjected to a potentiostatic hold test at 400 mV for 48 hours. Figures 8a, 8b and 8c show, respectively, the current output from beginning to end of testing for the MEAs prepared with 60 wt% of ionomer with ethanol, 50 wt% with isopropyl alcohol and 50 wt% with methanol.

MEAs with ethanol and methanol showed the highest beginning of test (BOT) current density outputs (BOT = 0.491 $A \cdot cm^{-2}$ and 0.454 $A \cdot cm^{-2}$, respectively). Isopropyl alcohol had the lowest current output (BOT = 0.295 $A \cdot cm^{-2}$) although at the end of test (EOT) current output suffered a slight decay (EOT = 0.277 $A \cdot cm^{-2}$), translating into a loss of 0.38 $mA \cdot h^{-1}$. Contrarily, ethanol and methanol had considerably higher performance decays (EOT = 0.425 $A \cdot cm^{-2}$ and 0.387 $A \cdot cm^{-2}$, respectively) and a similar current loss of 1.38 and 1.40 $mA \cdot h^{-1}$, respectively.

As mentioned, a larger micropore surface area leads to higher initial performance and higher degradation decay. In fact, the high electrode capacitance of the MEAs prepared with ethanol and methanol can be interpreted as high surface area, and the obtained results seem to agree with this statement. The MEA prepared with isopropyl alcohol had the lowest electrode capacitance, the lowest BOT performance and the slowest current decay. Isopropyl alcohol might cause less catalyst oxidation by H_2O_2 due to the lower active area available, but results are inconclusive. Serov *et al.* (2016) tested the same catalyst under similar experimental conditions. Through focused ion beam (FIB) sectioning they stated that at EOT the MEAs suffered loss of connectivity and electrode/MEA structure collapse (34). Considering their findings and the above statement that high particle dispersion (high zeta-potential) leads to ionomer straining and breakage of proton conducting pathways, another hypothesis for the lower decay with isopropyl alcohol is the "thicker" pathways it promotes. If flooding and carbon corrosion occur throughout the stability testing, less initial ionomer straining could lead to a slower connectivity loss and less current decay.

In order to understand the influence of micropore flooding, demetallation and carbon corrosion by H_2O_2 formation in the stability of MEAs fabricated by the method of this work, further research is needed. Carbon oxidation accelerated test protocols allow to determine if the failure mode is caused by catalyst corrosion or by MEA structure collapse, indicating a solvent impact on the carbon corrosion resistance of the catalyst. FIB sectioning would allow to analyze MEA roughness, porosity and connectivity differences throughout the stability test. While the catalyst used in this work was recently referred to as demonstrating high stability (34), electrode fabrication must be optimized towards achieving high performing PEMFCs with high stability for several working hours.

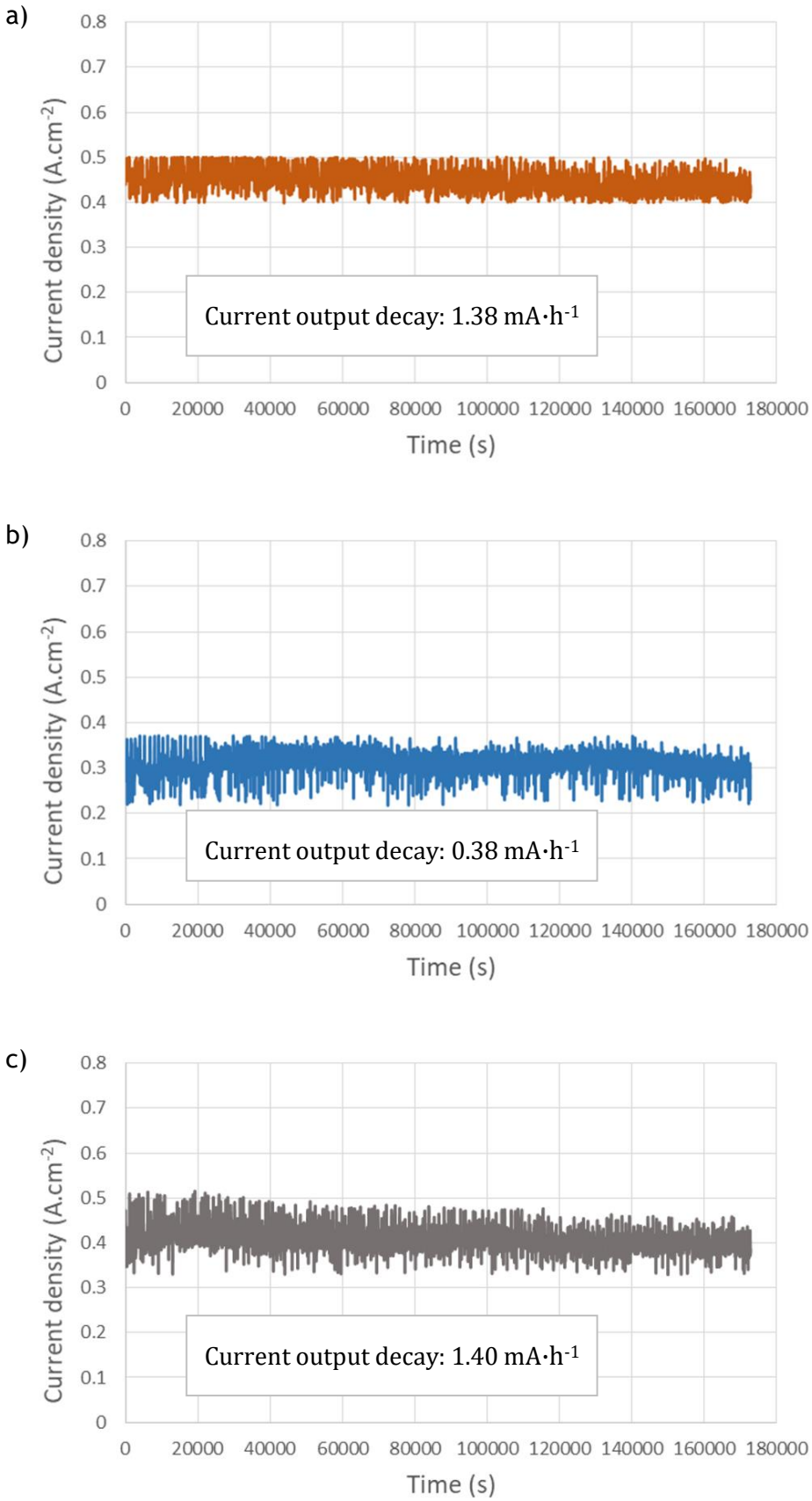

Figure 8. Potentiostatic hold test at 400 mV for MEAs prepared with: a) 60 wt% ionomer with Ethanol; b) 50 wt% ionomer with Isopropyl alcohol; c) 50 wt% ionomer with Methanol.

5 Conclusions

This work aimed to develop an optimized ink suspension of a PGM-free catalyst by optimizing the ionomer/catalyst ratio and solvent used during the ink preparation stage, alongside the development of an optimized MEA. In this study, ethanol, isopropyl alcohol and methanol were tested as solvents. Ionomer content applied in the ink suspensions was either 60, 50 or 40 wt%.

A clear correlation between fuel cell performance and ionomer content and used solvent was found. Zeta-Potential analysis allowed to comprehend the impact of particle dispersion in the electrode performance, in which there seems to exist an "optimal" balance between excessive or insufficient particle dispersion.

CV and EIS electrochemical analysis gave insights regarding electrode capacitance and active area, and impedance in the activation and ohmic regions, respectively. According to the obtained results for ethanol and isopropyl alcohol, it seems that a higher ionomer content leads to a higher electrode capacitance and power densities. However, methanol seems to promote the opposite tendency. In order to comprehend the causes behind this condition, further studies are needed. Of the three tested solvents, methanol prompted the lowest obtained impedances. At low current densities this can be explained by the higher dielectric constant of methanol and the zeta-potential range for the prepared inks, which leads to an "optimal" active surface area in the electrode.

Stability testing revealed that higher performing MEAs also suffer higher degradation rates, yet the main responsible mechanism remains unknown.

For the solvent types and ionomer contents tested in this work, use of methanol at 50 wt% of ionomer content produced the highest peak power density (0.229 $W \cdot cm^{-2}$), which is comparable to recent state of the art PGM-free catalysts. Even so, stability performance continues to be a problem requiring further research and development of novel catalysts/electrode constructions. Furthermore, in order to fully understand solvent influence on the ionomer dispersion through the CL, further analysis (such as TEM and FIB) is warranted.

6 Assessment of the work done

This work aimed to develop an optimized ink suspension of a Fe-N-C catalyst, specifically by optimizing the ionomer/catalyst ratio and solvent type used during the ink preparation stage. Performance differences between MEAs were discussed in terms of the active surface area of the catalyst, determined by CV, and by the proton resistance through the CL, measured by EIS. Furthermore, Zeta-Potential measurements were run for the produced inks to analyse the stability and agglomeration of the catalyst particles in the suspension.

All of the stated objectives were accomplished during the projected period of time. Nevertheless, due to the recent Covid-19 pandemic and mandatory quarantine, a more thorough analysis was not possible. In this sense, while some ionomer contents and solvents were tested, other wt% ratios and types of solvent under consideration were set aside. Different casting techniques such as hand spraying and analysing the effect of freeze drying on the performance were not possible. Also, further characterization techniques such as TEM were not pursued. Transmission line modelling of the obtained EIS results was not completed, owing to the impossibility of working with the DLR supervisor due to the restricted number of persons allowed per laboratory. Finally, the optimized ink suspension and MEA assembly were not tested with another Fe-N-C catalyst to confirm their transversality with other PGM-free catalysts.

7 References

1. Day C, Day G. Climate change, fossil fuel prices and depletion: The rationale for a falling export tax. Economic Modelling. 2017;63:153-60.

2. Gowrisankaran G, Reynolds SS, Samano M. Intermittency and the value of renewable energy. Journal of Political Economy. 2016;124(4):1187-234.

3. Dicks AL, Rand DA. Fuel cell systems explained: John Wiley & Sons; 2018.

4. O'hayre R, Cha S-W, Colella W, Prinz FB. Fuel cell fundamentals: John Wiley & Sons; 2016.

5. Winter C-J. Hydrogen energy—Abundant, efficient, clean: A debate over the energy-system-of-change. International journal of hydrogen energy. 2009;34(14):S1-S52.

6. Lemke C, Grueger F, Arnhold O. MELY: Market Model for Water Electrolysis—Electrolysis' Economic Potential given its Technological Feasibility. Energy Procedia. 2015;73:59-68.

7. Shao M, Chang Q, Dodelet J-P, Chenitz R. Recent advances in electrocatalysts for oxygen reduction reaction. Chemical reviews. 2016;116(6):3594-657.

8. Thompson ST, Papageorgopoulos D. Platinum group metal-free catalysts boost cost competitiveness of fuel cell vehicles. Nature Catalysis. 2019;2(7):558-61.

9. Yin X, Lin L, Chung HT, Babu SK, Martinez U, Purdy GM, et al. Effects of MEA fabrication and ionomer composition on fuel cell performance of PGM-free ORR catalyst. ECS Transactions. 2017;77(11):1273.

10. Wu G, Swaidan R, Li D, Li N. Enhanced methanol electro-oxidation activity of PtRu catalysts supported on heteroatom-doped carbon. Electrochimica Acta. 2008;53(26):7622-9.

11. He B-L, Zhou Y-K, Zhou W-J, Dong B, Li H-L. Preparation and characterization of ruthenium-doped polypyrrole composites for supercapacitor. Materials Science and Engineering: A. 2004;374(1-2):322-6.

12. Makharia R, Mathias MF, Baker DR. Measurement of catalyst layer electrolyte resistance in PEFCs using electrochemical impedance spectroscopy. Journal of The Electrochemical Society. 2005;152(5):A970-A7.

13. Hunter RJ. Zeta potential in colloid science: principles and applications: Academic press; 2013.

14. Demuren A, Edwards RL. Modeling Proton Exchange Membrane Fuel Cells—A Review. 50 Years of CFD in Engineering Sciences: Springer; 2020. p. 513-47.

15. Wu H-W. A review of recent development: Transport and performance modeling of PEM fuel cells. Applied Energy. 2016;165:81-106.

16. Kirubakaran A, Jain S, Nema R. A review on fuel cell technologies and power electronic interface. Renewable and Sustainable Energy Reviews. 2009;13(9):2430-40.

17. Chen Z, Dodelet J-P, Zhang J. Non-noble metal fuel cell catalysts: John Wiley & Sons; 2014.

18. Wang Y, Chen KS, Mishler J, Cho SC, Adroher XC. A review of polymer electrolyte membrane fuel cells: Technology, applications, and needs on fundamental research. Applied energy. 2011;88(4):981-1007.

19. Majlan E, Rohendi D, Daud WRW, Husaini T, Haque M. Electrode for proton exchange membrane fuel cells: a review. Renewable and Sustainable Energy Reviews. 2018;89:117-34.

20. So M, Ohnishi T, Park K, Ono M, Tsuge Y, Inoue G. The effect of solvent and ionomer on agglomeration in fuel cell catalyst inks: Simulation by the Discrete Element Method. International Journal of Hydrogen Energy. 2019;44(54):28984-95.

21. Bvumbe TJ, Bujlo P, Tolj I, Mouton K, Swart G, Pasupathi S, et al. Review on management, mechanisms and modelling of thermal processes in PEMFC. Hydrogen and Fuel Cells. 2016;1(1):1-20.

22. Shao M. Electrocatalysis in fuel cells: a non-and low-platinum approach: Springer Science & Business Media; 2013.

23. Gong K, Osepowicz NE, Livaich E, Desouza A, Brown P. Fuel cell assembly including multiple flow capacities in a condensation zone. Google Patents; 2019.

24. Pilatowsky I, Romero RJ, Isaza C, Gamboa S, Sebastian P, Rivera W. Cogeneration Fuel Cells–Air Conditioning Systems. Cogeneration Fuel Cell-Sorption Air Conditioning Systems: Springer; 2011. p. 103-20.

25. Kumar A, Dixit CK. Methods for characterization of nanoparticles. Advances in nanomedicine for the delivery of therapeutic nucleic acids: Elsevier; 2017. p. 43-58.

26. Duclos L, Svecova L, Laforest V, Mandil G, Thivel P-X. Process development and optimization for platinum recovery from PEM fuel cell catalyst. Hydrometallurgy. 2016;160:79-89.

27. Duclos L, Lupsea M, Mandil G, Svecova L, Thivel P-X, Laforest V. Environmental assessment of proton exchange membrane fuel cell platinum catalyst recycling. Journal of Cleaner Production. 2017;142:2618-28.

28. Jaouen F, Proietti E, Lefèvre M, Chenitz R, Dodelet J-P, Wu G, et al. Recent advances in non-precious metal catalysis for oxygen-reduction reaction in polymer electrolyte fuel cells. Energy & Environmental Science. 2011;4(1):114-30.

29. Holewinski A, Idrobo J-C, Linic S. High-performance Ag–Co alloy catalysts for electrochemical oxygen reduction. Nature chemistry. 2014;6(9):828.

30. Stacy J, Regmi YN, Leonard B, Fan M. The recent progress and future of oxygen reduction reaction catalysis: A review. Renewable and Sustainable Energy Reviews. 2017;69:401-14.

31. Sabatier P. Hydrogénations et déshydrogénations par catalyse. Berichte der deutschen chemischen Gesellschaft. 1911;44(3):1984-2001.

32. Wang G, Osmieri L, Star AG, Pfeilsticker J, Neyerlin K. Elucidating the Role of Ionomer in the Performance of Platinum Group Metal-free Catalyst Layer via in situ Electrochemical Diagnostics. Journal of The Electrochemical Society. 2020;167(4):044519.

33. Cetinbas FC, Ahluwalia RK. Agglomerates in polymer electrolyte fuel cell electrodes: Part II. Transport characterization. Journal of The Electrochemical Society. 2018;165(13):F1059.

34. Serov A, Workman MJ, Artyushkova K, Atanassov P, McCool G, McKinney S, et al. Highly stable precious metal-free cathode catalyst for fuel cell application. Journal of Power Sources. 2016;327:557-64.

35. Huang X, Zhao Z, Cao L, Chen Y, Zhu E, Lin Z, et al. High-performance transition metal–doped Pt3Ni octahedra for oxygen reduction reaction. Science. 2015;348(6240):1230-4.

36. Shao M, Shoemaker K, Peles A, Kaneko K, Protsailo L. Pt monolayer on porous Pd– Cu alloys as oxygen reduction electrocatalysts. Journal of the American Chemical Society. 2010;132(27):9253-5.

37. Gasteiger HA, Kocha SS, Sompalli B, Wagner FT. Activity benchmarks and requirements for Pt, Pt-alloy, and non-Pt oxygen reduction catalysts for PEMFCs. Applied Catalysis B: Environmental. 2005;56(1-2):9-35.

38. Ishihara A, Imai H, Ota Ki. Transition Metal Oxides, Carbides, Nitrides, Oxynitrides, and Carbonitrides for O2 Reduction Reaction Electrocatalysts for Acid PEM Fuel Cells. Non-Noble Metal Fuel Cell Catalysts. 2014:183-204.

39. Osmieri L. Transition metal–nitrogen–carbon (M–N–C) catalysts for oxygen reduction reaction. Insights on synthesis and performance in polymer electrolyte fuel cells. ChemEngineering. 2019;3(1):16.

40. Jia Q, Ramaswamy N, Hafiz H, Tylus U, Strickland K, Wu G, et al. Experimental observation of redox-induced Fe–N switching behavior as a determinant role for oxygen reduction activity. Acs Nano. 2015;9(12):12496-505.

41. Martinez U, Komini Babu S, Holby EF, Chung HT, Yin X, Zelenay P. Progress in the Development of Fe-Based PGM-Free Electrocatalysts for the Oxygen Reduction Reaction. Advanced Materials. 2019;31(31):1806545.

42. Shui J, Chen C, Grabstanowicz L, Zhao D, Liu D-J. Highly efficient nonprecious metal catalyst prepared with metal–organic framework in a continuous carbon nanofibrous network. Proceedings of the National Academy of Sciences. 2015;112(34):10629-34.

43. Wan X, Liu X, Li Y, Yu R, Zheng L, Yan W, et al. Fe–N–C electrocatalyst with dense active sites and efficient mass transport for high-performance proton exchange membrane fuel cells. Nature Catalysis. 2019;2(3):259-68.

44. Banham D, Choi JY, Kishimoto T, Ye S. Integrating PGM-Free Catalysts into Catalyst Layers and Proton Exchange Membrane Fuel Cell Devices. Advanced Materials. 2019;31(31):1804846.

45. Ratso S, Sahraie NR, Sougrati MT, Käärik M, Kook M, Saar R, et al. Synthesis of highly-active Fe–N–C catalysts for PEMFC with carbide-derived carbons. Journal of Materials Chemistry A. 2018;6(30):14663-74.

46. Chung HT, Cullen DA, Higgins D, Sneed BT, Holby EF, More KL, et al. Direct atomic-level insight into the active sites of a high-performance PGM-free ORR catalyst. Science. 2017;357(6350):479-84.

47. Serov A, Shum AD, Xiao X, De Andrade V, Artyushkova K, Zenyuk IV, et al. Nano-structured platinum group metal-free catalysts and their integration in fuel cell electrode architectures. Applied Catalysis B: Environmental. 2018;237:1139-47.

48. Hatzell KB, Dixit MB, Berlinger SA, Weber AZ. Understanding inks for porous-electrode formation. Journal of Materials Chemistry A. 2017;5(39):20527-33.

49. Liu J, Talarposhti MR, Asset T, Sabarirajan DC, Parkinson DY, Atanassov P, et al. Understanding the Role of Interfaces for Water Management in Platinum Group Metal-Free Electrodes in Polymer Electrolyte Fuel Cells. ACS Applied Energy Materials. 2019;2(5):3542-53.

50. Osmieri L, Mauger S, Ulsh M, Neyerlin KC, Bender G. Use of a segmented cell for the combinatorial development of platinum group metal-free electrodes for polymer electrolyte fuel cells. Journal of Power Sources. 2020;452:227829.

51. Ahluwalia R, Wang X, Osmieri L, Peng J, Chung H, Neyerlin KC. Performance of Polymer Electrolyte Fuel Cell Electrodes with Atomically Dispersed (AD) Fe-CN ORR Catalyst. Journal of The Electrochemical Society. 2019;166(14):F1096-F104.

52. Kongkanand A, Mathias MF. The priority and challenge of high-power performance of low-platinum proton-exchange membrane fuel cells. The journal of physical chemistry letters. 2016;7(7):1127-37.

53. Shao Y, Dodelet JP, Wu G, Zelenay P. PGM-Free Cathode Catalysts for PEM Fuel Cells: A Mini-Review on Stability Challenges. Advanced Materials. 2019;31(31):1807615.

54. Proietti E, Jaouen F, Lefèvre M, Larouche N, Tian J, Herranz J, et al. Iron-based cathode catalyst with enhanced power density in polymer electrolyte membrane fuel cells. Nature communications. 2011;2(1):1-9.

55. Banham D, Ye S. Current status and future development of catalyst materials and catalyst layers for proton exchange membrane fuel cells: an industrial perspective. ACS Energy Letters. 2017;2(3):629-38.

56. Du L, Luo L, Feng Z, Engelhard M, Xie X, Han B, et al. Nitrogen–doped graphitized carbon shell encapsulated NiFe nanoparticles: A highly durable oxygen evolution catalyst. Nano Energy. 2017;39:245-52.

57. Choi CH, Choi WS, Kasian O, Mechler AK, Sougrati MT, Brüller S, et al. Unraveling the Nature of Sites Active toward Hydrogen Peroxide Reduction in Fe-N-C Catalysts. Angewandte Chemie International Edition. 2017;56(30):8809-12.

58. Prabhakaran V, Wang G, Parrondo J, Ramani V. Contribution of Electrocatalyst Support to PEM Oxidative Degradation in an Operating PEFC. Journal of The Electrochemical Society. 2016;163(14):F1611-F7.

59. Chenitz R, Kramm UI, Lefèvre M, Glibin V, Zhang G, Sun S, et al. A specific demetalation of Fe–N 4 catalytic sites in the micropores of NC_Ar+ NH 3 is at the origin of the initial activity loss of the highly active Fe/N/C catalyst used for the reduction of oxygen in PEM fuel cells. Energy & Environmental Science. 2018;11(2):365-82.

60. Yang L, Larouche N, Chenitz R, Zhang G, Lefèvre M, Dodelet J-P. Activity, performance, and durability for the reduction of oxygen in PEM fuel cells, of Fe/N/C electrocatalysts obtained from the pyrolysis of metal-organic-framework and iron porphyrin precursors. Electrochimica Acta. 2015;159:184-97.

61. Wang YC, Zhu PF, Yang H, Huang L, Wu QH, Rauf M, et al. Surface fluorination to boost the stability of the Fe/N/C cathode in proton exchange membrane fuel cells. ChemElectroChem. 2018;5(14):1914-21.

62. Martinez U, Babu SK, Holby EF, Zelenay P. Durability challenges and perspective in the development of PGM-free electrocatalysts for the oxygen reduction reaction. Current Opinion in Electrochemistry. 2018;9:224-32.

63. Banham D, Kishimoto T, Zhou Y, Sato T, Bai K, Ozaki J-i, et al. Critical advancements in achieving high power and stable nonprecious metal catalyst–based MEAs for real-world proton exchange membrane fuel cell applications. Science advances. 2018;4(3):eaar7180.

64. Liu G, Li X, Lee J-W, Popov BN. A review of the development of nitrogen-modified carbon-based catalysts for oxygen reduction at USC. Catalysis Science & Technology. 2011;1(2):207-17.

65. Herranz J, Jaouen F, Lefèvre M, Kramm UI, Proietti E, Dodelet J-P, et al. Unveiling N-protonation and anion-binding effects on Fe/N/C catalysts for O2 reduction in proton-exchange-membrane fuel cells. The Journal of Physical Chemistry C. 2011;115(32):16087-97.

66. Zhang G, Chenitz R, Lefèvre M, Sun S, Dodelet J-P. Is iron involved in the lack of stability of Fe/N/C electrocatalysts used to reduce oxygen at the cathode of PEM fuel cells? Nano Energy. 2016;29:111-25.

67. Choi CH, Baldizzone C, Grote JP, Schuppert AK, Jaouen F, Mayrhofer KJ. Stability of Fe-N-C catalysts in acidic medium studied by operando spectroscopy. Angewandte Chemie International Edition. 2015;54(43):12753-7.

68. Choi CH, Lim H-K, Chung MW, Chon G, Sahraie NR, Altin A, et al. The Achilles' heel of iron-based catalysts during oxygen reduction in an acidic medium. Energy & environmental science. 2018;11(11):3176-82.

69. Nosaka Y, Ohtaka K, Ohguri N, Nosaka AY. Detection of OH radicals generated in polymer electrolyte membranes of fuel cells. Journal of The Electrochemical Society. 2011;158(4):B430.

70. Orfanidi A, Rheinländer PJ, Schulte N, Gasteiger HA. Ink solvent dependence of the ionomer distribution in the catalyst layer of a PEMFC. Journal of The Electrochemical Society. 2018;165(14):F1254.

71. Welch C, Labouriau A, Hjelm R, Orler B, Johnston C, Kim YS. Nafion in dilute solvent systems: Dispersion or solution? ACS Macro Letters. 2012;1(12):1403-7.

72. Ngo TT, Yu TL, Lin H-L. Influence of the composition of isopropyl alcohol/water mixture solvents in catalyst ink solutions on proton exchange membrane fuel cell performance. Journal of Power Sources. 2013;225:293-303.

73. Osmieri L, Videla AHM, Specchia S. The use of different types of reduced graphene oxide in the preparation of Fe-NC electrocatalysts: capacitive behavior and oxygen reduction reaction activity in alkaline medium. Journal of Solid State Electrochemistry. 2016;20(12):3507-23.